The acquisition of clinically relevant amoxicillin resistance in *Streptococcus pneumoniae* requires ordered horizontal gene transfer of four loci

Paddy S. Gibson[1], Evan Bexkens[1], Sylvia Zuber[1], Lauren A. Cowley[2], Jan-Willem Veening[1,*]

[1] Department of Fundamental Microbiology, Faculty of Biology and Medicine, University of Lausanne, Biophore Building, CH-1015 Lausanne, Switzerland

[2] Department of Biology & Biochemistry, Milner Centre for Evolution, University of Bath, Claverton Down Campus, Bath BA2 7AY, United Kingdom

[*]Correspondence to Jan-Willem Veening: Jan-Willem.Veening@unil.ch, tel: +41 (0)21 6925625, Twitter handle: @JWVeening

Abstract

Understanding how antimicrobial resistance spreads is critical for optimal application of new treatments. In the naturally competent human pathogen *Streptococcus pneumoniae*, resistance to β-lactam antibiotics is mediated by recombination events in genes encoding the target proteins, resulting in reduced drug binding affinity. However, for the front-line antibiotic amoxicillin, the exact mechanism of resistance still needs to be elucidated. Through successive rounds of transformation with genomic DNA from a clinically resistant isolate, we followed amoxicillin resistance development. Using whole genome sequencing, we showed that multiple recombination events occurred at different loci during one round of transformation. We found examples of non-contiguous recombination, and demonstrated for the first time that this can occur through multiple D-loop formation from one donor DNA molecule or by the uptake of multiple DNA fragments. We also show that the final minimum inhibitory concentration differs depending on recipient genome, and the sampled fitness landscape. Finally, through back transformations of mutant alleles and fluorescently labelled penicillin (bocillin-FL) binding assays, we show that *pbp1a*, *pbp2b*, *pbp2x*, and *murM* are the main resistance determinants for amoxicillin resistance, and that the order of allele uptake matters. We conclude that recombination events are complex, and that this complexity contributes to the highly diverse genotypes of amoxicillin-resistant pneumococcal isolates.

Introduction

Genomic plasticity through frequent and large-scale recombination drives the evolution of antibiotic resistance in *Streptococcus pneumoniae* (the pneumococcus) (Salvadori et al., 2019). This naturally competent member of the human nasopharyngeal commensal microbiota opportunistically causes otitis media as well as severe invasive diseases such as pneumonia, bacteremia, and meningitis (O'Brien et al., 2009; Shak et al., 2013). Despite conjugate vaccine introduction, the species remains an important human pathogen, as vaccine-escape and antibiotic resistant variants constantly arise (Croucher et al., 2011; Wyres et al., 2013).

Variants occur primarily through natural transformation and homologous recombination of DNA from strains or closely related species that occupy the same niche, such as *S. mitis* and *S. oralis* (Croucher et al., 2012; Dowson et al., 1993; Sibold et al., 1994). One case study showed more than 7% of the genome had been transferred between two pneumococcal strains during the polyclonal infection of a pediatric patient over three months (Hiller et al., 2010). Early studies of transformation in the pneumococcus showed uptake of fragments ranging from 2-6 Kb (Gurney and Fox, 1968), but cell-to-cell contact was found to facilitate transfer of long DNA fragments (Cowley et al., 2018), and recombinant regions as large as 30 – 50 Kb in length have been observed in clinically relevant lineages such as PMEN-1 (Croucher et al., 2011; Wyres et al., 2013, 2012). Events such as these have played a significant role in shaping the pneumococcal pangenome (Donati et al., 2010).

Natural competence is activated when the competence stimulating peptide (CSP) interacts with the ComDE two-component system (Straume et al., 2015) (Figure 1). Phosphorylated ComE initiates a positive feedback loop for CSP production and activates transcription of the genes encoding the alternative sigma factor *comX* (Martin et al., 2013; Slager et al., 2019; Ween et al., 1999). ComX then activates transcription of the late *com* genes necessary for DNA uptake and recombination. Exogenous DNA uptake is mediated by a type IV-like pilus (ComGC), which brings double-stranded molecules within reach of the endonuclease EndA (Bergé et al., 2013; Laurenceau et al., 2013). This enzyme randomly nicks the strands in multiple locations, and a single strand is transported into the cell by ComFA and ComEC, while the non-transported strand is degraded (Lacks and Greenberg, 1976; Lacks and Neuberger, 1975; Rosenthal and Lacks, 1980). RecA and the transformation-dedicated DNA processing

63 protein A (DprA) are essential for single-stranded DNA (ssDNA) uptake without degradation
64 (Attaiech et al., 2011). Although not fully understood, DprA and RecA are thought to
65 polymerize on ssDNA upon cell entry, initiating the homology search, while additional DNA
66 molecules are then bound by multiple SsbB proteins protecting them from degradation by
67 endogenous nucleases (Attaiech et al., 2011; Morrison et al., 2007). It has been hypothesized
68 that the accumulation of stable ssDNA-SsbB eclipse complexes in the cytoplasm enables
69 successive recombination events during one competence window, increasing genetic
70 plasticity (Attaiech et al., 2011). Sequestered ssDNA can then be accessed by the
71 transformation-dedicated DNA processing protein A (DprA), which mediates the loading of
72 RecA onto the pre-synaptic filament (Lisboa et al., 2014; Mortier-Barrière et al., 2007;
73 Quevillon-Cheruel et al., 2012). DprA is also involved in competence shut-off, blocking
74 phosphorylated ComE specific transcriptional activation, although secondary control may
75 come from ComX and RpoD sigma factor competition (Martin et al., 2013; Mirouze et al.,
76 2013; Piotrowski et al., 2009; Weng et al., 2013).

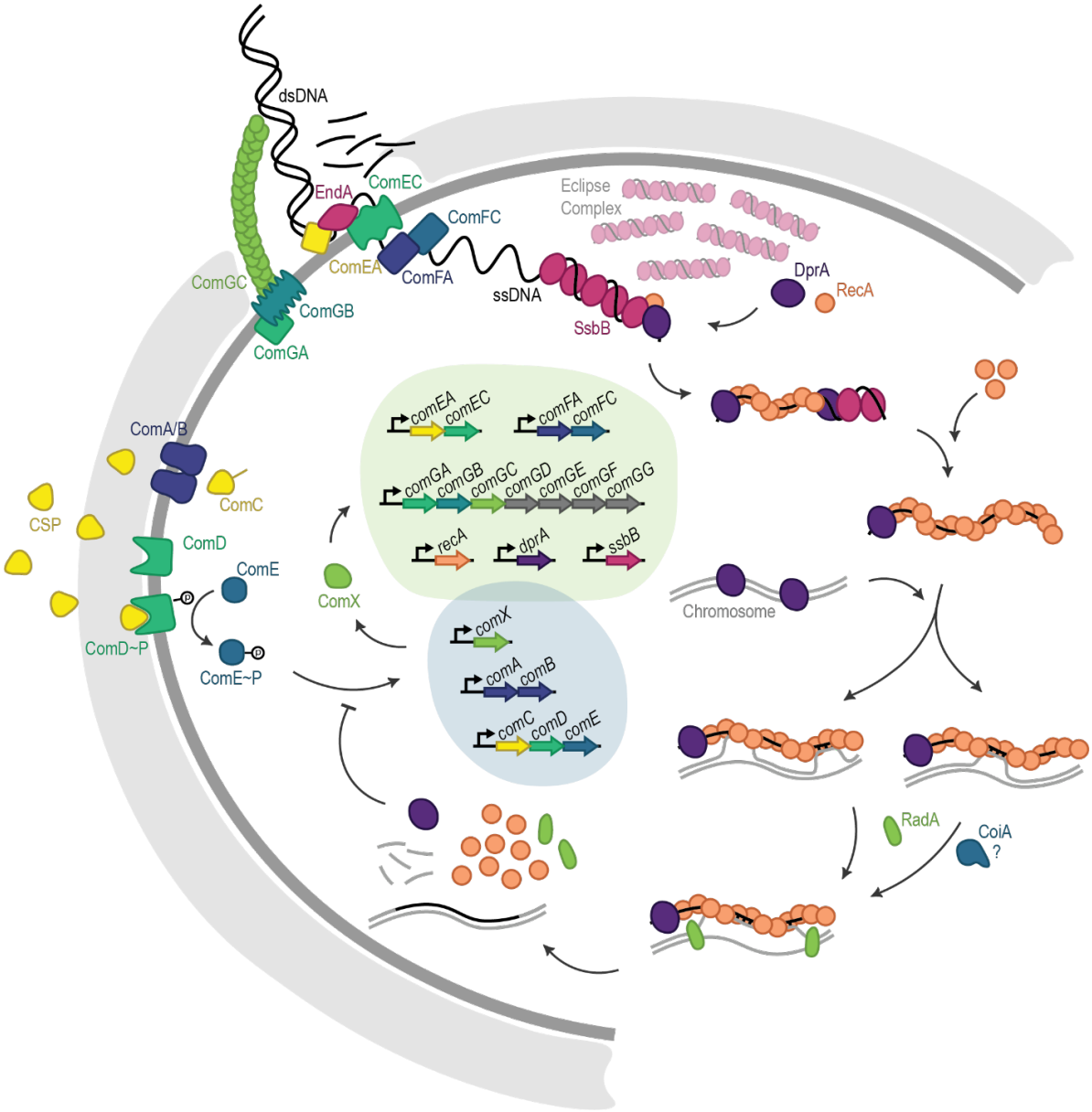

77

Figure 1: DNA uptake and recombination during natural competence in *Streptococcus pneumoniae*. Schematic overview of the regulatory steps required for the pneumococcus to uptake and recombine extracellular DNA. Competence is activated when CSP interacts with the ComDE two-component system, where phosphorylated ComE activates transcription of ComX and other early competence genes (darker grey bubble). This results in a positive feedback loop, where ComC is produced, then modified and exported from the cell by ComA/B as CSP. Meanwhile, ComX activates transcription of late competence genes, including the type IV-like pilus (ComGC), which brings DNA within reach of endonuclease EndA. EndA performs random nicks, then degrades one strand as the other is pulled into the cell and associated with DprA, RecA, and SsbB, to protect from degradation (exact mechanism not fully understood). DprA mediates loading of RecA onto SsbB-ssDNA eclipse complexes to form the presynaptic filament which then searches the chromosome for homology. RecA-ssDNA filaments may interact with the chromosome at multiple points, while successful base pairing between incoming and chromosomal DNA facilitates strand invasion and exchange. The helicase RadA facilitates D-loop extension, and CoiA is essential for successful recombination during transformation, although its exact role is not known. DprA is also involved in competence shut off, through blocking phosphorylation of ComE.

78

Competence is tightly controlled, with expression of most genes turned off within 20 minutes of CSP induction, providing a small window for DNA uptake and recombination (Alloing et al., 1998). To accelerate homology detection, the RecA-ssDNA presynaptic filament has been shown to interact with the chromosome in 3-dimensional space at multiple points of contact (Forget and Kowalczykowski, 2012; Wiktor et al., 2021; Yang et al., 2020). Displacement-loop (D-loop) formation is facilitated by base pairing between the chromosome and the ssDNA molecule, within the two DNA-binding sites of RecA (Bell and Kowalczykowski, 2016; Torres et al., 2019). Eight consecutive bases must be successfully paired before the DNA-DNA interaction is stabilized and strand exchange can occur (Hsieh et al., 1992; Mazin and Kowalczykowski, 1996). In *S. pneumoniae*, D-loop extension is promoted by RadA (DnaB-type helicase) which helps to unwind chromosomal DNA, extending recombination over long genomic distances (Marie et al., 2017), and while its function is not known, CoiA is essential for successful recombination (Desai and Morrison, 2007; Mortier-Barrière et al., 2007). Although initial testing is highly stringent, once crossover has started and the region of complementation is extended, stringency decreases, allowing some mismatches thereby increasing desirable genetic variation (Danilowicz et al., 2015). This is aided by the generalized mismatch repair system in *S. pneumoniae* (hex) which is not induced during competence (Claverys and Lacks, 1986), is only able to identify mismatches in the donor-recipient heteroduplex before D-loop resolution (Claverys and Lacks, 1986; Gasc et al., 1989), (Gasc et al., 1989) and is easily overwhelmed by excess mismatches (Humbert et al., 1995).

Penicillin binding proteins (PBPs) are key β-lactam resistance determinants and are essential for bacterial cell wall synthesis by catalyzing the transglycosylation (TG) and transpeptidation (TP) reactions responsible for peptidoglycan (PGN) formation (Scheffers and Pinho, 2005). While highly conserved in penicillin (PEN) sensitive strains, PBPs of resistant isolates are highly variable, with up to 10% of amino acid changes (Hakenbeck et al., 2012). Significant amounts of this variation was recently confirmed to be acquired from *S. mitis* (Kalizang'oma et al., 2021). These large-scale changes alter the structure of the active sites, reducing β-lactam binding affinity (Hakenbeck et al., 2012). Amoxicillin (AMX) is the first line oral antibiotic prescribed for bacterial lower respiratory tract infections. AMX resistant strains first appeared in the mid-90s in the United States and France (Doern et al., 1996; Doit et al., 1999) and are currently on the rise in Spain, a phenomenon which correlates with increased usage of oral

110 AMX/clavulanic acid (Càmara et al., 2018). Sequencing of *pbp* alleles from susceptible and
111 resistant strains implicated mutations in *pbp2x*, *pbp2b* and *pbp1a* (Cafini et al., 2006; Chesnel
112 et al., 2005; du Plessis et al., 2002; Kosowska et al., 2004). However, no SNP or block of SNPs
113 in any one *pbp*, when transferred to a susceptible strain, has been sufficient to confer
114 resistance in a susceptible strain (Hakenbeck et al., 1998; Kosowska et al., 2004). This is not
115 entirely surprising, as the transpeptidase activity of PBPs is an essential function, and
116 modifications to the active site are likely to have deleterious effects which need to be
117 compensated for (Albarracín Orio et al., 2011). One mechanism of fitness compensation
118 appears to be through substitutions in MurM, which results in abnormally high proportions
119 of branched muropeptides in the cell wall (Filipe et al., 2002; Filipe and Tomasz, 2000; Garcia-
120 Bustos and Tomasz, 1990; Smith and Klugman, 2001). Other non-target proteins which have
121 been implicated in resistance include CpoA (Grebe et al., 1997) and CiaH (Guenzi et al., 1994).

122 Although multiple residues in Pbp1a, Pbp2x, and Pbp2b were found to be under positive
123 selection in AMX resistant isolates (Stanhope et al., 2008), only substitutions in Pbp2b are
124 repeatedly linked to AMX resistant isolates, specifically a block of ten substitutions in the 590-
125 641 region in the TP domain (Cafini et al., 2006; du Plessis et al., 2002; Kosowska et al., 2004).
126 However, transformation of *pbp2x*, *pbp2b*, and *pbp1a* alleles to AMX susceptible strain R6 did
127 not recreate the AMX resistance of the donor strain, and the addition of *murM* had no effect.
128 Only when genomic DNA was used could the original resistance level be achieved, indicating
129 the role of a non-*pbp* or *murM* resistance determinant (du Plessis et al., 2002), or unknown
130 epistatic interactions (Arnold et al., 2018). Interestingly, other studies have found a
131 correlation between *murM* mutations and AMX resistance, although their presence
132 depended on the *pbp2b* allele (Cafini et al., 2006; Càmara et al., 2018). Taken together, these
133 studies strongly suggest the existence of multiple routes to AMX resistance and imply a tight
134 link in the roles of Pbp2b and MurM in the mechanisms.

135 To study recombination and the development of AMX resistance in the pneumococcus in
136 more detail and identify possible evolutionary routes towards AMX resistance, we
137 sequentially transformed genomic DNA from a resistant clinical isolate (serotype 11A, ST6521,
138 German National Reference Centre for Streptococci 2017, SN75752) into two different
139 recipient strains coming from different clonal complexes (serotype 2 D39V and serotype 4
140 TIGR4). Whole genome sequencing showed recipient-dependent, genome-wide mutation

141 uptake. In addition to identifying the necessary determinants for AMX resistance, we found a
142 strong tendency towards the order of *pbp* and *murM* allele uptake. Long read Pacbio
143 sequencing excluded a role for DNA methylation or genomic rearrangements or movement
144 of genetic mobile elements as resistance determinants. We also investigated non-contiguous
145 recombination and propose a model for how these complex events occur. To conclude, we
146 show that the uptake of four alleles from a resistant strain (*pbp2X*, *pbp2B*, *pbp1A* and *murM*),
147 in a specific order, is required and sufficient for clinically relevant resistance development
148 towards amoxicillin in sensitive *S. pneumoniae*.
149

150 **Results**

151 ***Serial transformation with AMX-R genomic DNA increased AMX MIC***

152 In order to understand the sequence of recombination events leading to the development of
153 AMX resistance, a susceptible *S. pneumoniae* strain D39V was transformed in two successive
154 rounds with genomic DNA originating from AMX resistant clinical isolate 11A followed by
155 selection on AMX (Figure 2A, Table 1). Ten colonies were isolated in the first round (0.03
156 µg/mL AMX). The MICs of these strains ranged from 0.047 – 0.125 µg/mL, 4 – 10 times that
157 of wild-type D39V (Figure 2B, Table S1).

158 The second round of transformation resulted in 100 strains with MICs from 0.25 to 2 µg/mL
159 (Figure 2B), lower than the donor strain, and a third round of transformation did not increase
160 the MIC further. Interestingly, five of the ten lineages had seven or more strains with MICs of
161 1 µg/mL or higher. In contrast, the AMR37 lineage resulted in MICs from 0.25 – 0.5 µg/mL,
162 with one exception at 2 µg/mL. These lineage-dependent differences in AMX MIC range (p =
163 5×10^{-4}, Fisher's Exact Test) suggested that mutations acquired in the first round contributed
164 to the recombination events which occurred in the second round, and thus to the MICs of the
165 resulting strains.
166

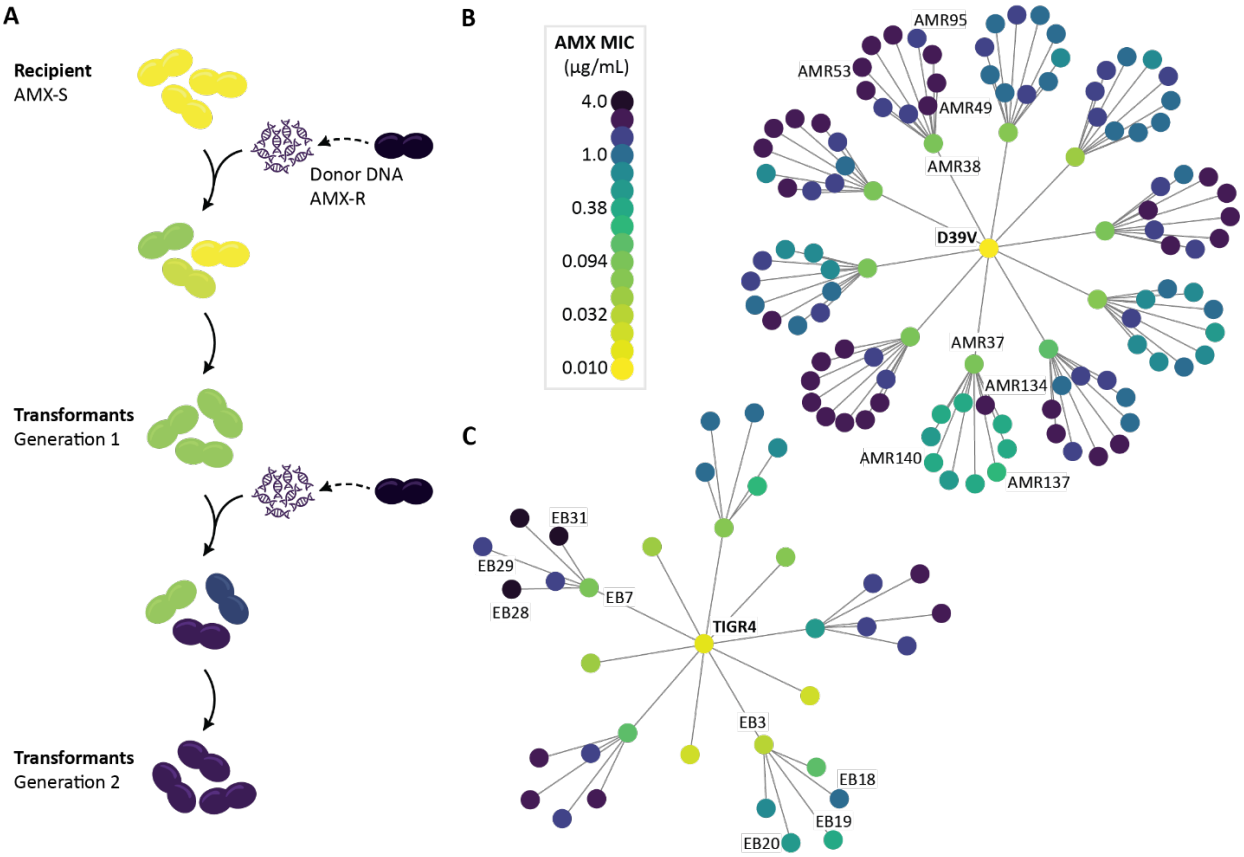

167

Figure 2: **Transformation as an experimental tool to track the evolutionary path to AMX resistance**. **(A)** Experimental design. Susceptible D39V and TIGR4 were transformed with genomic DNA from an AMX-R clinical isolate then selected on AMX (first round on 0.03 µg/mL and second round on 0.17 – 0.3 µg/mL, depending on MIC of the recipient strain). Isolated transformants with increased MICs were then subjected to a second round of transformation. **(B)** Pedigree chart of recombinant strains derived from D39V, and **(C)** from TIGR4. Color represents AMX MIC. Strains which were sequenced and used throughout the study are labelled.

168 Similar lineage-dependent MIC patterns were seen when TIGR4 was used as the recipient
169 strain (p = 1.00x10^{-3}, Fisher's Exact Test) (Figure 2B). Here, the AMX MICs of the first-
170 generation ranged from 0.023 – 0.5 µg/mL, with one strain showing a more than 30-fold
171 increase from wild-type TIGR4. In the second-generation, three recombinant strains reached
172 the same MIC as the donor strain (4 µg/mL), suggesting potential key differences in the
173 recipient strain genomes, or deleterious epistatic effects of AMX resistance mutations which
174 affected resistance development through recombination.

175

176 ***Cell lysis upon AMX treatment correlated with PBP affinities***

177 To test whether transformed strains phenocopy the donor with regards to AMX resistance,
178 phase contrast microscopy with an AMX concentration above the recipient MICs (1 μg/mL)
179 was performed. A complete stall in growth was observed for both recipient strains and first-
180 generation recombinant AMR38, with mild to severe lysis after 6 hrs of treatment (Figure 3A).
181 In contrast, donor strain 11A grew to form a microcolony in this AMX concentration, while
182 second-generation AMR53 grew more slowly and with abnormally elongated cells (Figure 3A).
183 To test whether the increased resistance of AMR53 is related to alterations in the affinity of
184 the PBPs towards AMX, we performed Bocillin-Fl labelling. Bocillin-Fl is a fluorescently
185 labelled penicillin derivative that binds all six PBPs of *S. pneumoniae* (Zhao et al., 1999), and
186 the intensity of labelling can be used as a proxy for the affinity of the PBP for β-lactam
187 antibiotics (Kocaoglu et al., 2015). All six PBPs of D39V and TIGR4 had a high affinity for the
188 fluorescently labelled penicillin (Figure3B). Interestingly, TIGR4 showed some evidence of
189 Pbp1A degradation products that bound Bocillin-Fl with high affinity even though it is xx%
190 identical to D39V Pbp1A. In contrast, 11A showed an altered PBP pattern, where PBP2b and
191 Ppb1a showed complete loss of affinity, and Pbp2x was labelled more faintly and migrated
192 more slowly (Figure 3B).

193 Both first- and second-generation recombinants demonstrated a loss of affinity of Pbp2b and
194 Pbp2x for Bocillin-FL, with PBP1a in AMR53 also showing reduced affinity, and potentially
195 some degradation (Figure 3B). Together, these characterizations demonstrate that
196 transformed recipients phenocopy the donor AMX resistant strain and have acquired PBPs
197 with reduced affinity towards bocillin-FL.

198

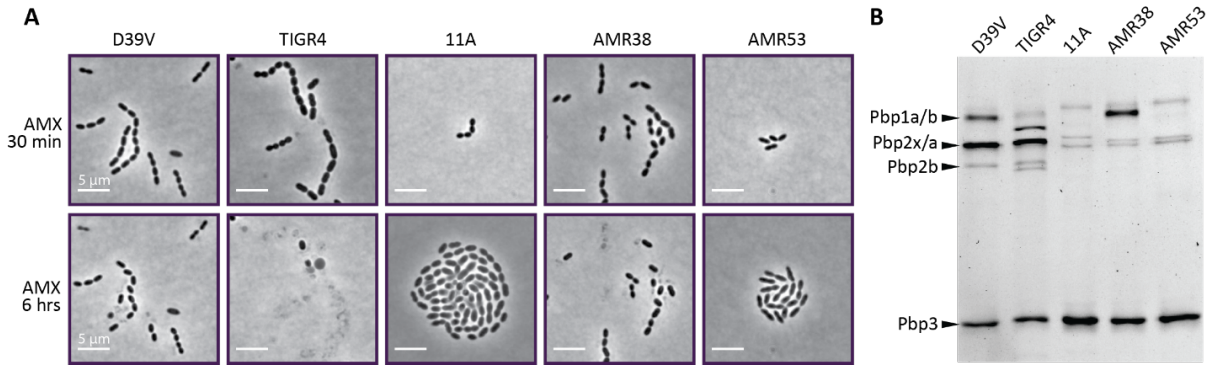

Figure 3: Phenotypic characterization of key strains used in this study. (**A**) Phase-contrast snapshots of recipient strains D39V and TIGR4, donor strain 11A, and recombinant strains AMR38 (generation 1) and AMR53 (generation 2) on C+Y agarose pads after 30 minutes and 6 hours of treatment with 1 µg/mL AMX. This concentration was above MIC for D39V, TIGR4, and AMR38, and lead to a complete stall in growth and partial lysis. Donor strain 11A grew well in this AMX concentration, although some heterogeneity in cell shape could be observed. Although lower than the AMX MIC for AMR53, this strain showed decreased growth and abnormally elongated cells, indicating cells were stressed. Scale bar is 5 µm. (B) Bocillin-FL binding patterns for the same five strains. Expected PBP band sizes for D39V are shown on the left. Image of Coomassie stained gel can be found in Figure S1)

199 ***Recombination events clustered around resistance-associated loci***

200 Recombinant strains were Illumina sequenced to ~600-fold mean coverage. To be able to
201 accurately map recipient to donor, we also performed long-read PacBio sequencing followed
202 by short-read polishing on the 11A donor and TIGR4 recipient (an accurate genome map was
203 already available for D39V (Slager et al., 2018)). Recombination was detected using SNPs, as
204 described in Cowley et al. (2018). On average 0.38 % ± 0.22 % of the donor genome was
205 transferred during a single transformation event, and the total percentage transferred after
206 two rounds was 0.80 ± 0.05%. Although higher numbers of recombination events were
207 detected in the D39V dataset, the average event length was larger in the TIGR4 dataset (D39V
208 0.79 Kb and TIGR4 2.29 Kb, Table S3 and S4), resulting in similar total amounts of donor
209 genome transfer after two rounds of transformation (D39V 0.79 ± 0.23%, TIGR4 0.80 ± 0.16%,
210 Table S3 and S4). Of note, the longest recorded recombination fragment was 4.00 Kb for D39V
211 and 12.52 Kb for TIGR4.

212 Recombination events clustered around key loci for pneumococcal β-lactam resistance in
213 both datasets; *pbp2x*, *pbp2b*, *pbp1a* and *murM* (Figure 4A and 5C). SNPs were also found at
214 closely located loci, likely due to linkage. In the D39V strains, there was extensive
215 recombination at distantly located sites. Examples include *ptvABC*, associated with

216 vancomycin tolerance (Liu et al., 2017), and *murT*, which performs an amidation step essential
217 for peptidoglycan crosslinking (Figueiredo et al., 2012; Münch et al., 2012).
218

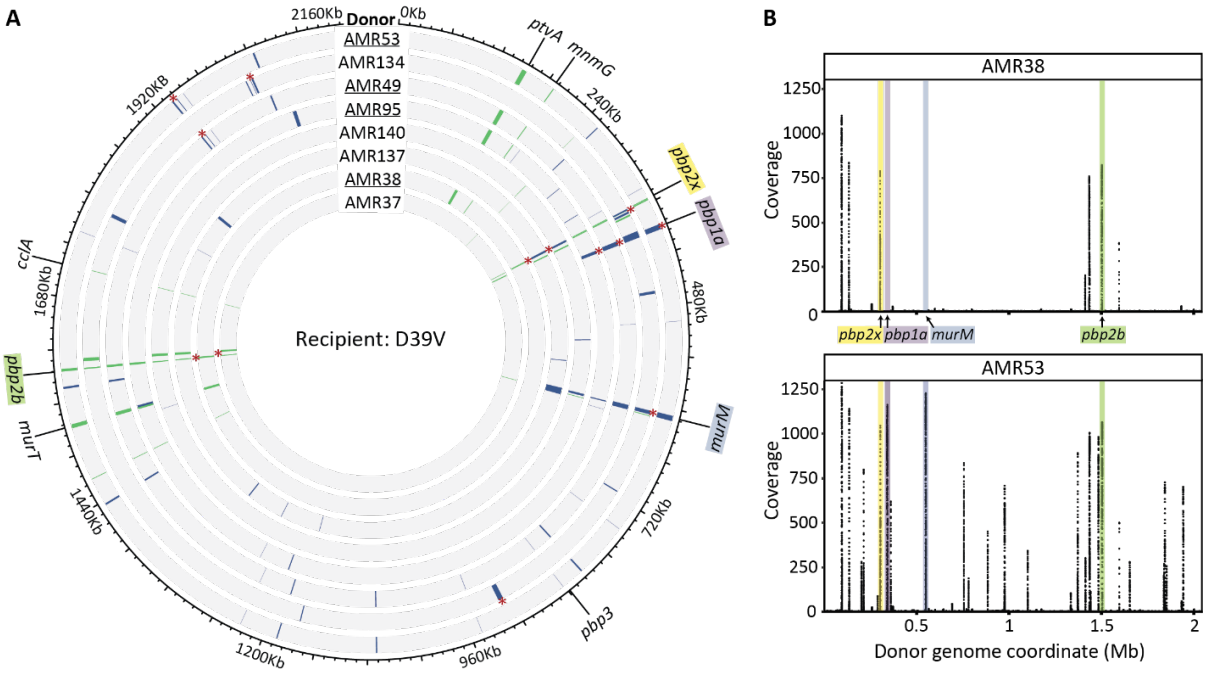

219

Figure 4: **Widespread transformation and uptake of 11A donor DNA in recipient D39V upon AMX selection**. **(A)** Circos plot with detected recombination events in D39V derived strains, arranged from lowest to highest MIC from the center. AMR38 and all derived strains are underlined, AMR37 and all derived strains are not. Grey indicates the sequences matches that of the recipient D39V, while recombination events are colored. Events acquired in the first round of transformation are shown in green, in the second round in blue, and lengths were increased to aid in visualization (see Table S3 for a list of all detected events). Recombination events determined to be non-contiguous are marked with (*). Non-contiguous events detected in the first-generation were removed from the data set on the second-generation strains, so are not marked. **(B)** Coverage of reads mapped competitively to the donor genome and plotted by coordinate beginning at the origin. Recombination events cluster at known β-lactam resistance determinants, *pbp2x*, *pbp2b*, *murM*, and *pbp1a*.

220 In contrast, of the six total recombination loci in the TIGR4 dataset, only three were located
221 distally from the *pbp* and *murM* genes, and all were detected based on the presence of very
222 few SNPs.
223 We hypothesised that differences in recombination patterns could have arisen from reduced
224 similarity with the donor genome, however comparing total shared and unique SNPs did not
225 suggest major differences in variability between the two recipient genomes (Figure 5A). When
226 considering variation around key loci, we saw that the TIGR4 *pbp2b* region was more
227 divergent from the donor than D39V. The quality of donor DNA used may have also played a
228 role. Together, these results demonstrate that regardless of the recipient strain, four loci are

229 consistently acquired in high AMX resistant recombinants, namely *pbp2x*, *pbp2b*, *pbp1a* and
230 *murM* (Figure 5B).
231 Structural variation and base modification detection with PacBio sequencing revealed no
232 major structural changes or differences in methylated motifs in the D39V recombinant
233 strains. However, a local rearrangement was identified at the *hsdS-creX* locus in EB7, EB28,
234 and EB29. In this region, spontaneous reshuffling of *hsdS* genes by CreX results in different
235 methyltransferase specificity of the type I restriction modification system SpnD39III (Feng et
236 al., 2014; Manso et al., 2014; Slager et al., 2018). TIGR4 was found to be predominantly in the
237 B-configuration, EB7 and EB29 in the D-configuration, and EB28 in the C-configuration, while
238 all D39V-derived strains and 11A were mostly in the F-configuration. Differences in
239 methylated motifs have transcriptomic consequences (Manso et al., 2014), however MIC
240 differences among these recombinants can largely be explained by SNPs in key loci for β-
241 lactam resistance.
242

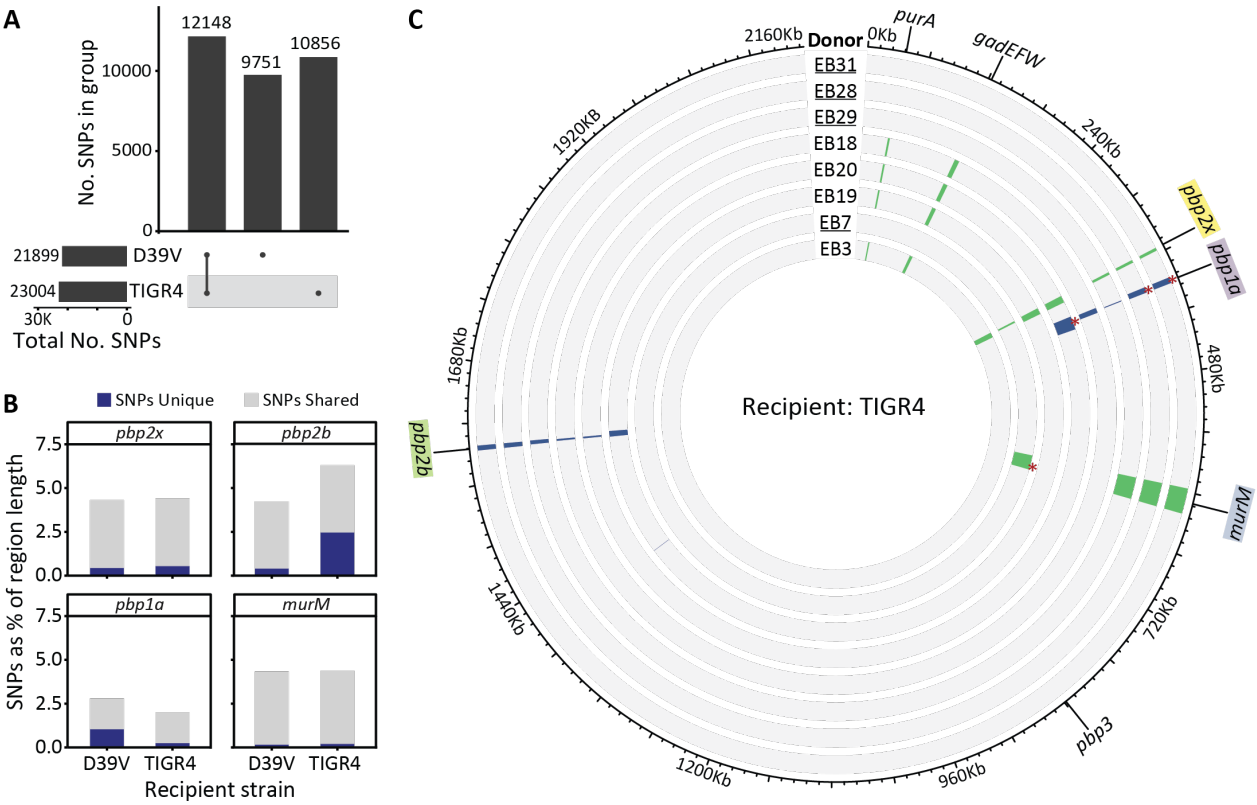

243

Figure 5: Uptake of four donor fragments is sufficient for AMX resistance in TIGR4. (A) Upset plot of shared and unique SNPs between each recipient and the donor. This shows that a total of 12148 SNPs from the 11A donor DNA were acquired in both the D39V and TIGR4 donors. **(B)** SNP counts in pbp/murM genes, including 5 Kb up- and downstream. Number of SNPs unique to each recipient are shown in blue, and shared in light grey. **(C)** Circos plot showing detected recombination events in TIGR4 derived strains, arranged from lowest to highest

MIC from inside to out. EB7 and all derived strains are underlined, EB3 and all derived strains are not. Grey indicates the sequences matches that of the recipient D39V, while recombination events are colored. Events acquired in the first round of transformation are shown in green, and in the second round in blue, and lengths were increased to aid in visualization (see Table S3 for a list of all detected events). Only six loci with recombination were identified in the entire data set, four of which are known β-lactam resistance determinants, *pbp2x*, *pbp2b*, *murM*, *pbp1a*.

244 ***Non-contiguous recombination events likely result from a single donor molecule***

245 Recombination is often thought of as a donor molecule forming a single D-loop at a
246 homologous site on the recipient chromosome, which is then expanded in both directions
247 until the requirement for homology is no longer met, at which point the interaction ends.
248 However, we detected recombination events from one round of transformation located very
249 close together on the chromosome, sometimes within the same gene but with separating
250 recipient SNPs, a motif reminiscent of clinically resistant mosaic *pbp* alleles. This has also been
251 noted previously in *in vitro* pneumococcal recombination studies and was hypothesized to
252 result from a single donor molecule (Croucher et al., 2012; Mortier-Barriere et al., 1997). To
253 determine if events were significantly close together, forming a single non-contiguous
254 recombination event, a bootstrapping approach was applied to the distances between novel
255 recombination events within the same strain (Croucher et al., 2012). We found 37 events
256 across all strains that could be amalgamated into single events under the assumptions of this
257 approach (Figure S2, Table S4).

258 In addition, using PCR amplified fragments of the *pbp2x-mraY* locus from 11A, we were able
259 to test, for the first time, whether non-contiguous recombination events occurred more
260 frequently when the template was provided as a single molecule, or as two overlapping
261 fragments. By ligating additional regions of non-homologous DNA, we also tested the effect
262 of molecule length on recombination.

263 Transformation efficiency increased with length of both the overall molecule, and the
264 homologous region (Figure 6A). This is in line with previous studies showing the importance
265 of molecule length and homology in pneumococcal transformation (Kurushima et al., 2020;
266 Morrison and Guild, 1972). The efficiencies of the short overlapping fragments were lower
267 than that of the long fragments, although increased slightly when transformed in
268 combination.

269 Recombination occurred in all colonies sequenced. When two overlapping fragments were
270 provided, uptake was often unequal, with either the upstream or downstream fragment
271 incorporated more often. Recombination of both fragments was observed in 1/20 cases and
272 was not observed when fragments were lengthened by non-homologous DNA (Figure S3A-H,
273 Table S7).

274 Non-contiguous recombination was detected in all conditions, although the frequency of
275 occurrence increased with length of homology (Figure 6C, Figure S3A-H, Table S7). It was
276 observed both when the template was given as a single long fragment, and as two overlapping
277 fragments.

278 Overall, the results suggested that the formation of multiple D-loops from a single template
279 molecule, or from multiple molecules, could lead to non-contiguous recombination events
280 (Figure 6D). However, given that longer homology and total molecule length increased the
281 efficiency of transformation partly by reducing strand degradation (Morrison and Guild,
282 1972), there may have been more opportunity for complex recombination patterns to occur
283 when longer fragments were taken up.

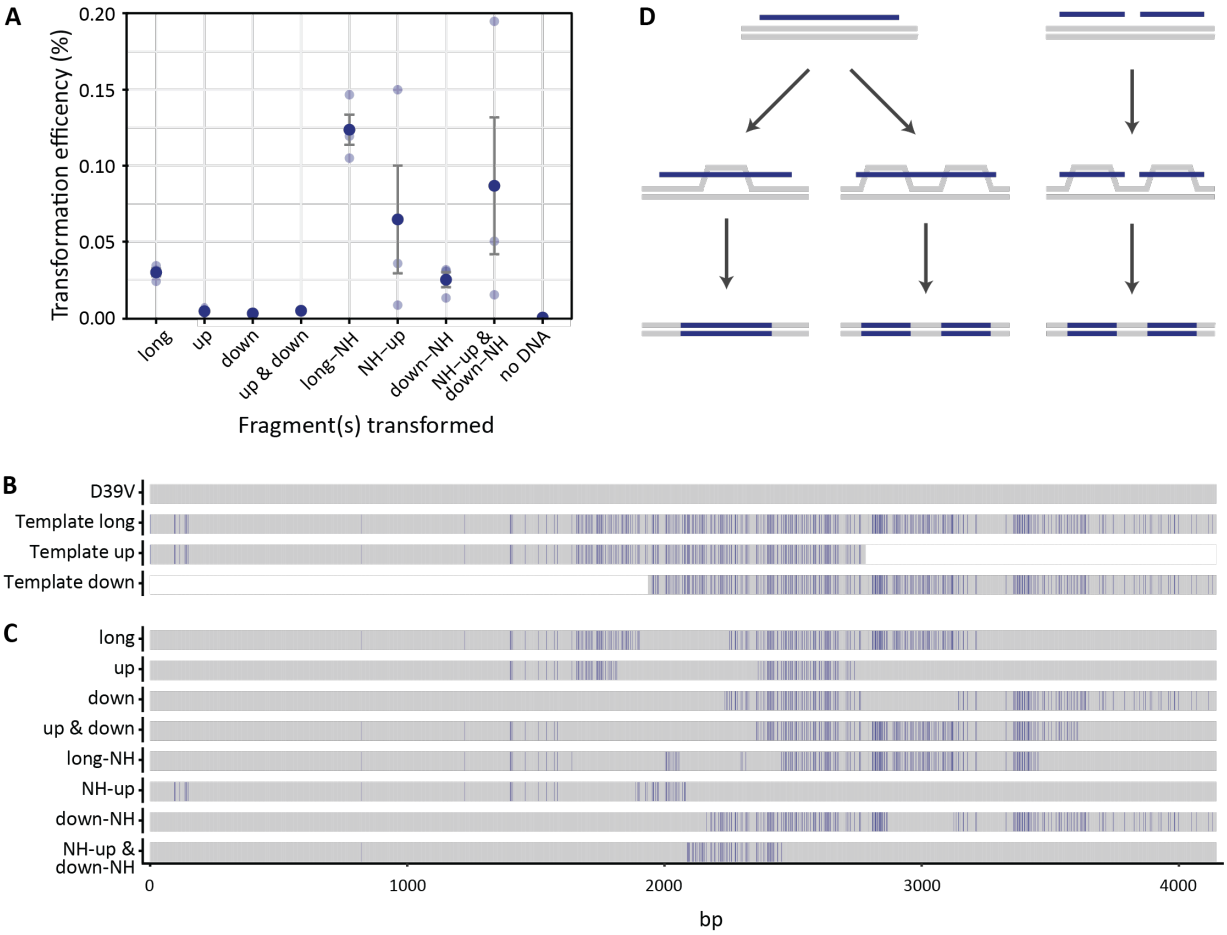

284

Figure 6: **Fragmented transformation of donor DNA predominantly originates from non-contiguous recombination events.** Three fragments were PCR amplified from the 11A strain *pbp2x* locus, one long 4.2 Kb fragment, and two overlapping short fragments (up 2837 Kb, and down 2260 Kb). In addition, the same fragments were ligated to stretches of non-homologous DNA, taking all total lengths to 6 Kb (long-NH, NH-up, and down-NH). **(A)** Efficiencies of transformation of fragments into D39V with selection on AMX (0.015 µg/mL). **(B)** Alignment of the homologous region of template fragments used in the experiment. Donor SNPs are shown in blue, while bases matching the recipient (D39V) are shown in grey. **(C)** Alignment of 4.2 Kb locus from colonies transformed with different fragments. Bases shared with donor but not with recipient are shown in blue. **(D)** Schematic showing hypothesized molecular mechanisms for non-contiguous and contiguous recombination. As shown in panel B, both events can take place, but based on transformation efficiencies, the process on the left with long donor DNA is more efficient.

285 ***AMX-R* pbp *and* murM *alleles are sufficient to explain AMX MICs***

286 Substitutions in all four proteins (PBP1a, PBP2b, PBP2x and MurM) were required to reach an
287 MIC close or equal to that of the donor strain (Figure S4, and Table S5), but the order of uptake
288 varied both stochastically, and depending on the recipient genome. The correlation between
289 allele uptake and MIC increase was consistent in the D39V background. First-generation
290 strains had mutations in *pbp2b* and *pbp2x*, the two essential PBPs for cell growth (Berg et al.,
291 2013). In the second-generation, all strains acquired mutations in *murM*, and those with MICs
292 higher than 1 µg/mL also had mutations in *pbp1a*. In TIGR4, *pbp2x* alleles were also acquired

293 in the first-generation, however *pbp2b* mutations only appeared after the second round of
294 transformation. Mutations in *murM* were inherited vertically in the EB7 lineage but were not
295 horizontally acquired by any EB3 descendant strains (Figure 4C). Although *murM* mutations
296 were not present in all strains with *pbp1a* modifications, strains with recombination events
297 at all four loci had higher MICs (Figure 2C). This indicated that *murM* mutations may be less
298 important for successful integration and selection for *pbp1a* mutations but are key for
299 expression of the AMX-R phenotype of the donor (Filipe et al., 2002; Filipe and Tomasz, 2000;
300 Garcia-Bustos and Tomasz, 1990; Smith and Klugman, 2001).
301 An experiment was designed to test whether the order of allele uptake in D39V recombinant
302 strains was crucial for AMX-R development, and if PBP and MurM substitutions alone were
303 sufficient to explain AMX MICs. Alleles of *pbp2x* and *pbp2b* from AMR37 (*pbp2x37*, *pbp2b37*)
304 and AMR38 (*pbp2x38*, *pbp2b38*) were transformed into D39V and selected on AMX. Strains
305 carrying either a recombinant *pbp2x* or *pbp2b* allele had E-test MICs up to 0.064 µg/mL.
306 However, when both *pbp* alleles were integrated (D39V$^{2x38\text{-}2b38}$), the E-test result equalled
307 that of the recombinant allele donor (Figure 7), suggesting that mutations outside these two
308 loci were not involved in the observed reduction in AMX susceptibility in the first-generation
309 strains.
310 To assess whether mutated *pbp2x* and *pbp2b* were critical for *murM* mutation uptake, D39V
311 was transformed with *murM* from both AMR53 (*murM53*) and AMR95 (*murM95*) and MICs
312 determined. Surprisingly, we were able to select for colonies with integration of the AMR53
313 *murM* allele (D39V^{M53}) resulting in an E-test result of 0.023 µg/mL, despite this protein not
314 being a direct target of AMX (Figure 7 and Figure 8A.B). The genome was sequenced, and no
315 spontaneous point mutations were identified in previously described resistance determinants
316 outside *murM* (Table S8). When transformed into the D39V$^{2x38\text{-}2b38}$, the E-test MICs reached
317 0.5 µg/mL and 0.38 µg/mL for AMR95 and AMR53 *murM* alleles (D39V$^{2x38\text{-}2b38\text{-}M95}$, D39V$^{2x38\text{-}}$
318 $^{2b38\text{-}M53}$), respectively. AMX susceptibility decreased substantially when all three genes were
319 mutated, however failed to reach the final MIC of the recombinant allele donor, indicating
320 the necessity of another resistance determinant (Figure 7).
321 *pbp1a* alleles from AMR53 and AMR95 (*pbp1a53*, *pbp1a95*) could not be successfully selected
322 on AMX when transformed into D39V, either alone or in conjunction with a *murM* allele from
323 the same donor. We instead transformed a construct where a kanamycin resistance cassette
324 was cloned behind *pbp1a*, with 1 Kb of homology up- and downstream. Growth in liquid

325 culture of the resulting strains at AMX 0.01 µg/mL was similar to D39V (Figure 8A.B).
326 Interestingly, successful integration occurred for both *pbp1a53* and *pbp1a95* when
327 transformed into D39V$^{2x38\text{-}2b38}$ (D39V$^{2x38\text{-}2b38\text{-}1a53}$, D39V$^{2x38\text{-}2b38\text{-}1a95}$), suggesting that a mutated
328 *murM* allele was not required for mutations in *pbp1a* to cause a selectable increase in AMX
329 MIC. However, substitutions in Pbp2x, Pbp2b, and Pbp1a alone were insufficient to replicate
330 the E-test results of the allele source strains (Figure 7).
331 We therefore transformed *murM* and *pbp1a* alleles from AMR53 and AMR95 into D39V$^{2x38\text{-}}$
332 ^{2b38} simultaneously, and found that selection was possible on higher concentrations of AMX
333 (1 µg/mL) than for either gene alone (0.2 µg/mL). The resulting strains (D39V$^{2x38\text{-}2b38\text{-}M53\text{-}1a53}$,
334 D39V$^{2x38\text{-}2b38\text{-}M95\text{-}1a95}$) had AMX resistance phenotypes matching those of AMR53 and AMR95,
335 with E-test results of 2 µg/mL and 1.5 µg/mL respectively (Figure 7).
336 The strains containing all four genes from AMR53 and AMR95 were whole genome sequenced
337 to check for spontaneous point mutations outside these loci. One non-synonymous mutation
338 in *glnA* (glutamine synthase type I) was found in both strains. Downregulation of *glnA* has
339 been linked to the pneumococcal penicillin stress response (el Khoury et al., 2017), but no
340 differences in AMX survival were observed in these strains compared to the allele donors
341 lacking the SNP.
342

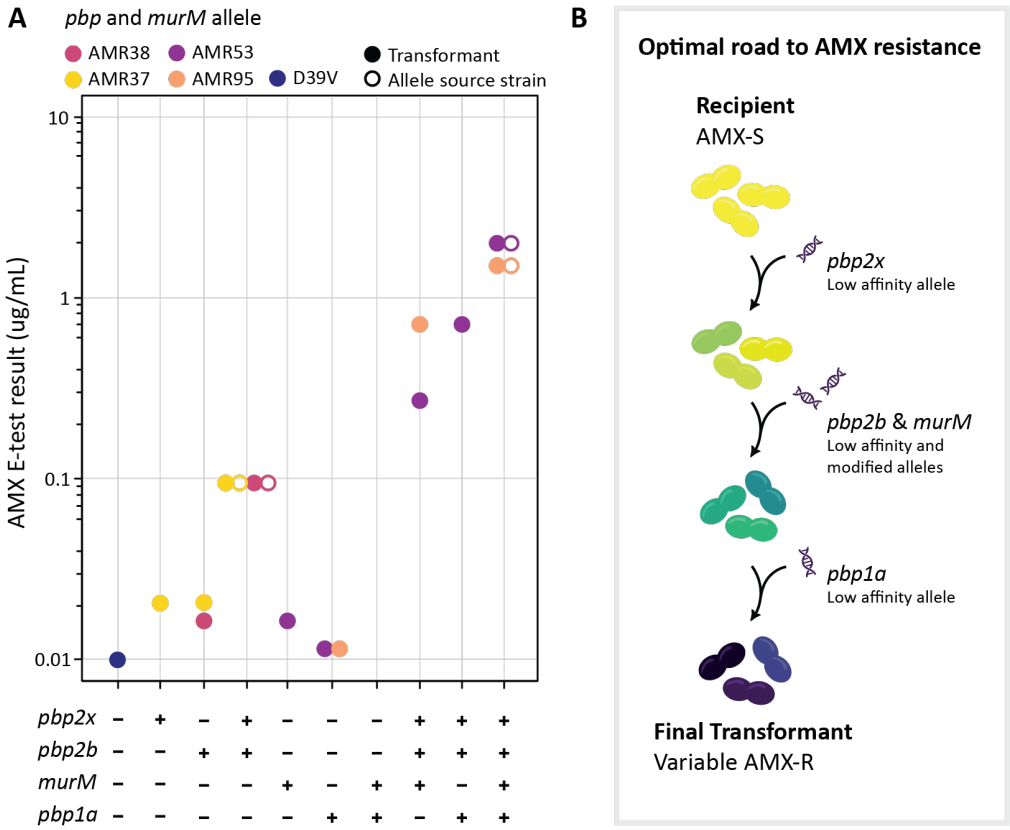

Figure 7: Uptake of mosaic *pbp1a*, *pbp2b*, *pbp2x* and *murM* is required and sufficient for clinically relevant amoxicillin resistance in *S. pneumoniae*. (A) AMX MICs determined by E-test for D39V transformant strains (solid circles) where *pbp* and *murM* alleles from different source strains (empty circles) were transformed in combination. Color shows allele source. (B) Schematic overview of the optimal road to AMX resistance development through horizontal gene transfer. Low affinity *pbp2x* was uptaken in the first round of transformation in both datasets, whereas donor *murM* and *pbp2b* alleles were acquired in the first or second round, depending on recipient and lineage. Low affinity *pbp1a* was recombined in the second round, and only found in strains with AMX MICs above 0.75 µg/mL. In principle uptake of low affinity and modified alleles could be achieved in a single (unlikely) or double step.

To quantify the affinities of resistant PBP alleles to β-lactam antibiotics, Bocillin-FL binding patterns were determined for allele swap strains and the source strains (Figure 8C.D). This confirmed that the recombinant PBPs had reduced penicillin binding affinities. For Pbp2b, both the AMR37 and AMR38 alleles resulted in almost complete loss of binding, and a band could not be quantified (Figure 8D). A large reduction in affinity was observed for Pbp2x38, larger than for Pbp2x37, which correlated to a small difference in growth at 0.1 µg/mL AMX between the two source strains (Figure 8A.B). This could be explained by 13 amino acid substitutions including S389L and T338A which were not present in the AMR37 allele but have previously been linked to reduced susceptibility to β-lactams (Kocaoglu et al., 2015; Kosowska et al., 2004).

354 Perhaps most interesting were the two low affinity Pbp1a alleles tested. In all strains
355 containing *pbp1a95* (AMR95 derived), reduced band intensity was observed in the
356 Pbp1a/Pbp1b size range, however, a faster migrating species was also detected. The *pbp1a95*
357 allele contained a spontaneous point mutation (not present in the 11A donor) causing a
358 premature stop codon. This resulted in the loss of 65 amino acids (of a total of 720) and put
359 the predicted size at 73.1 kDa instead of 79.6 kDa. Reduced intensity at the expected
360 Pbp1a/Pbp1b size range was also observed for the AMR53 allele (Pbp1a53) however, an
361 additional Bocillin-FL-tagged species which migrated slightly faster than expected was also
362 observed. The predicted protein length of Pbp1a53 is identical to D39V and the donor, with
363 no premature stop codons identified. The additional band may indicate some degradation of
364 this protein species, although the TP domain must still be available for Bocillin-FL binding.
365 Together, these experiments demonstrate that transfer of the *pbp2X*, *pbp2B*, *pbp1a* and
366 *murM* alleles of 11A into strain D39V is sufficient to explain the observed AMX resistance in
367 transformants obtained using chromosomal DNA.

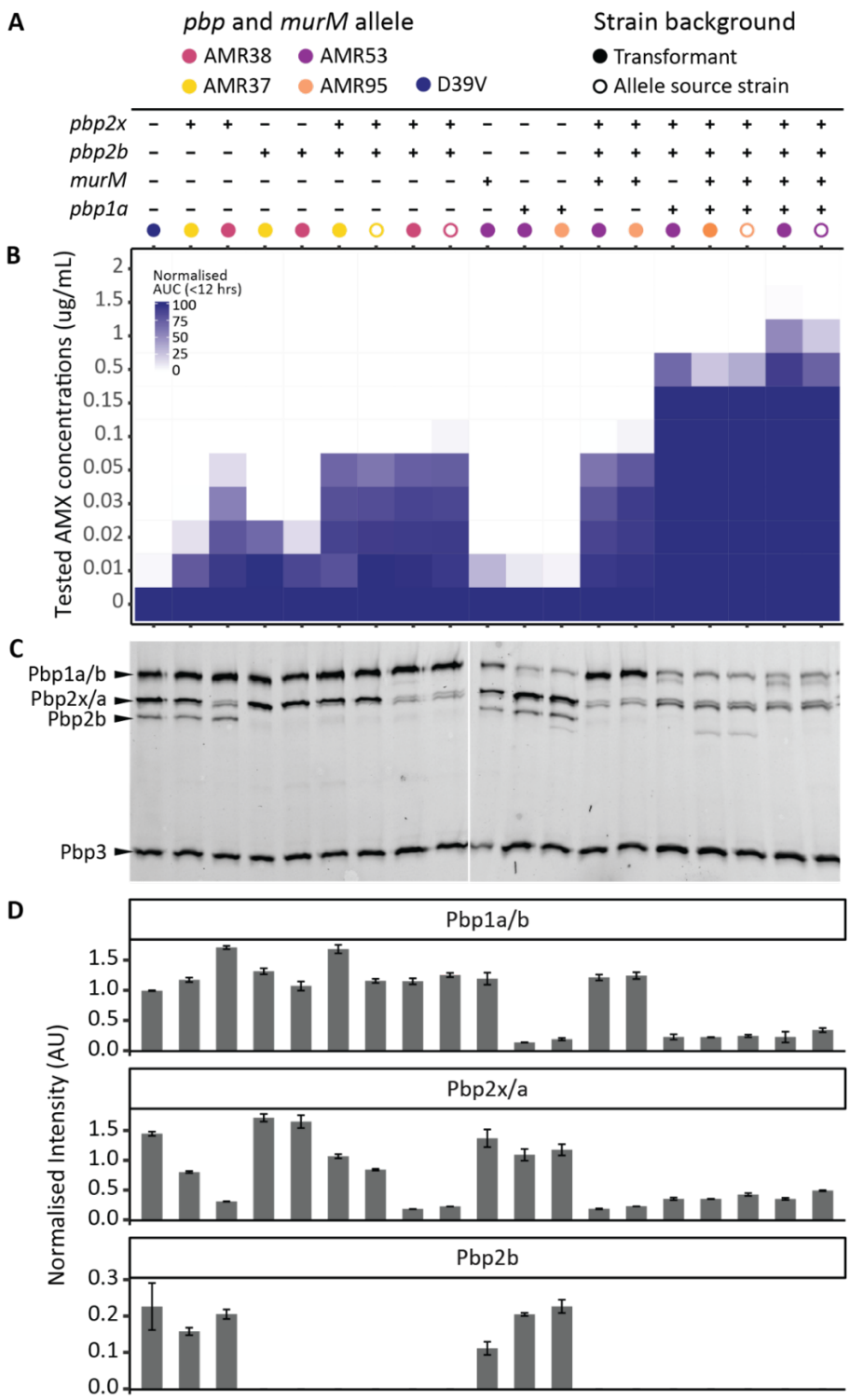

368

Figure 8: Recombinant PBP proteins visualized by PBP-bocillin binding affinities. Transformed AMX resistant strains produce mosaic PBPs with reduced affinity for Bocillin-FL. Each column shows the phenotypic characterization of one *pbp* and *murM* allele swap strain. **(A)** Table showing the presence (+) and absence (-) of alleles from different source strains (colour). Allele source strains are also included and are indicated by the unfilled circles. **(B)** Survival in different AMX concentrations quantified by determining the area under the growth curve (AUC) after 12 hours growth in AMX normalized by AUC in the absence of AMX. **(C)** Bocillin-FL binding affinity gel. **(D)** Intensity of bands corresponding to Pbp1a/b, Pbp2x/a, and Pbp2b, normalized by the intensity of the Pbp3 band of the same lane, as this allele remained unmodified in all strains.

369 ***High AMX resistance in the D39V comes at a significant fitness loss***

370 Of the 16 recombinant strains sequenced, only EB31 and EB28 from the TIGR4 collection had
371 the same AMX MIC as the donor strain, and a third round of transformation with gDNA into
372 AMR53 failed to increase the MIC. The only region of mutations that EB28 and EB31 had in
373 common that was not present in the highest MIC AMR strains, was a block of 10 mutations in
374 the 590-541 region of Pbp2b (Figure 9C, Table S5). To test whether these substitutions were
375 sufficient to explain the MIC difference, the *pbp2b* allele from EB31 (*pbp2b31*) was
376 transformed into AMR53 and AMR95. The AMX E-test scores for the resulting strains were
377 both 4-6 µg/mL. However, growth curves revealed a significant fitness loss, with a mean
378 maximum specific growth rate of 0.11 µ/h for AMR95 decreasing almost 100-fold to 0.0036
379 µ/h for AMR95^{2b31}, which was exacerbated by the presence of AMX (Figure 9B). In contrast,
380 AMR53^{2b31} grew almost 3-fold slower than AMR53 (AMR53 0.12 µ/h, AMR53^{2b31} 0.046 µ/h,
381 Figure 9B), but showed a lytic phenotype in stationary phase. Interestingly, this strain outgrew
382 the 11A donor in sublethal AMX concentrations (Figure 9A). The difference in growth rate
383 between AMR95^{2b31} and AMR53^{2b31} was likely explained by the truncated Pbp1a95 protein.
384 Significant modifications to the active sites of essential proteins often need to be
385 compensated for, which may be impacted by the sub-optimal performance of other proteins
386 in the system. Although the TP and TG domains of Pbp1a95 were intact, it is possible that the
387 loss of 65 amino acids from the C-terminal resulted in an overall reduction in function,
388 unrelated to its AMX binding affinity. Together, these experiments show that the D39V
389 lineage can reach high AMX resistance, but at a significant fitness cost in the absence of
390 compensation by substitutions in Pbp1A.

391

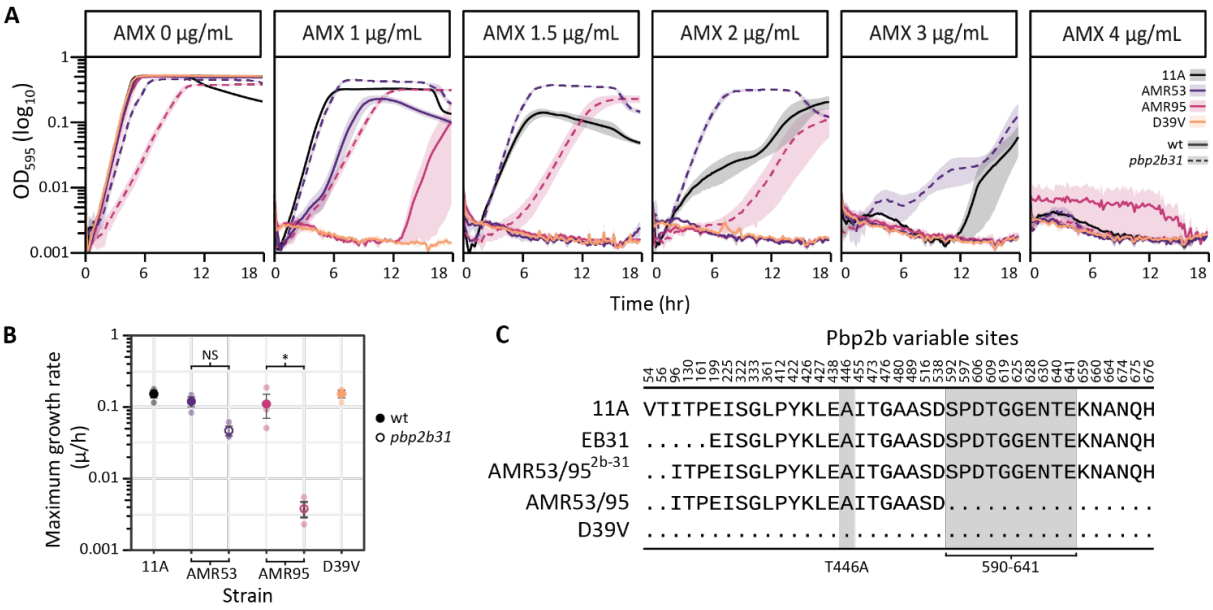

Figure 9: Ten substitutions in Pbp2b 590-641 region essential for high AMX resistance. (A) Growth of AMR53^{2b31} and AMR95^{2b31} (dotted lines) in different AMX concentrations. 11A, D39V, AMR53, and AMR95 (solid lines) are shown as controls. **(B)** Dot plot of maximum specific growth rates (µ/h) calculated from the AMX 0 µg/mL condition in triplicate (transparent circles). The mean for each strain is shown by an opaque circle, solid for wild-type (wt) strains and empty for AMR53^{2b31} and AMR95^{2b31}. Color denotes strain background. Significance was determined by one-way ANOVA with a Tukey correction for multiple testing. **(C)** Amino acid sites in pbp2b which differ from D39V for strains 11A, EB31, AMR53 (identical to AMR95), and AMR53^{2b31} (the result of transforming AMR53 or AMR95 with the EB31 pbp2b allele). Dots indicate the amino acid matches D39V, and key substitutions, T446A and a block of 10 between 590-641 (Cafini et al., 2006; du Plessis et al., 2002; Kosowska et al., 2004), are highlighted in grey.

Discussion

Natural competence and homologous recombination in *S. pneumoniae* allow for enormous genomic plasticity which contributes to the rapid development of vaccine-escape and antibiotic resistant isolates. In one round of transformation, more than 29 recombination events can occur in a single cell (Cowley et al., 2018), while events up to 50 Kb in length have been identified in clinical isolates (Wyres et al., 2013), allowing for significant remodelling at multiple loci simultaneously. Indeed, here we show a two-step sequential transformation experiment with up to 20 individual recombination events around the genome and lengths up to 13 Kb, resulting in an average donor genome transfer per step of 0.38%. This allows for huge genomic diversity, which, when placed under selective pressure, can lead to the rapid spread of antibiotic resistance-associated genotypes (Chewapreecha et al., 2014).

β-lactam resistance in the pneumococcus relies on DNA movement between closely related strains and species within the same niche, allowing tens of substitutions to accumulate in the

407 target proteins (Hakenbeck et al., 2012). For the front-line antibiotic AMX, resistance has been
408 previously associated with mutations in *pbp2x*, *pbp2b*, *pbp1a*, and *murM*, although the
409 relative importance of the changes in each locus is not well understood (Cafini et al., 2006;
410 Chesnel et al., 2005; du Plessis et al., 2002; Garcia-Bustos and Tomasz, 1990; Kosowska et al.,
411 2004; Smith and Klugman, 2001). We confirmed the requirement for mutations in all four
412 genes and showed that subtle differences between alleles could cause noticeable changes in
413 both AMX-dependent fitness and the penicillin-binding affinity of PBPs.
414 In addition, although a specific order of mutation uptake for penicillin resistance has been
415 demonstrated in both *Staphylococcus aureus* and the pneumococcus (Demerec, 1945;
416 Hotchkiss, 1951; Shockley and Hotchkiss, 1970), this has not yet been defined for AMX. Here,
417 we show that substitutions in Pbp2x are a critical first step for AMX resistance, perhaps
418 reflecting the protein's high affinity for the antibiotic (Kocaoglu et al., 2015)(Figure 7C), and
419 that the T338A substitution is required for resistance to fully develop. We also show that
420 mutations in both *pbp2b* and *murM* are essential intermediary steps, and that a modified
421 *pbp1a* allele is crucial for high-level AMX resistance. It is important to note that previous
422 studies have strongly implied the existence of multiple mechanisms of AMX resistance in *S.*
423 *pneumoniae*, associated with different *pbp2b* and *murM* alleles (Cafini et al., 2006; Càmara et
424 al., 2018), and that by using a single donor strain we were limited to the study of only one.
425 However, we confirmed that a previously described block of ten substitutions in the 590-641
426 region of the Pbp2b TP domain (Cafini et al., 2006; du Plessis et al., 2002; Kosowska et al.,
427 2004) was essential to reconstruct the AMX MIC of the serotype 11A ST6521 donor strain in
428 D39V and TIGR4. Perhaps most interestingly, we also show that the loss of 65 amino acids
429 from the C-terminus of Pbp1a results in a significant fitness cost in the presence of these
430 additional Pbp2b substitutions, highlighting the importance of interactions and fitness loss
431 compensation between essential cell-wall synthesis proteins (Albarracín Orio et al., 2011).
432 In addition to these definite experiments demonstrating the evolutionary route to clinical
433 AMX resistance, we show that non-contiguous recombination could result from either a
434 single, or multiple donor DNA molecules. It is easy to imagine a long ssDNA-RecA presynaptic
435 filament interacting with the chromosome at multiple points in the 3-dimensional cellular
436 space (Forget and Kowalczykowski, 2012; Yang et al., 2020)(Figure 1 model), which then
437 initiates the formation of several D-loops simultaneously as homologous DNA-DNA
438 interactions stabilize (Bell and Kowalczykowski, 2016; Hsieh et al., 1992; Mazin and

439 Kowalczykowski, 1996). On the other hand, SsbB coated ssDNA sequestered in the cytoplasm
440 could provide a pool from which multiple donor molecules homologous for the same
441 chromosomal region could be sourced (Attaiech et al., 2011). However, we also observed that
442 both transformation efficiency and non-contiguous event occurrence increased with length
443 of homology and total length of the donor molecule, suggesting that single donor molecule
444 events may simply be more likely. This concurs with the previous observation of transforming
445 DNA concentration-independent differences in recombination event density, which would
446 not have been expected under a multiple donor molecule hypothesis (Croucher et al., 2012).
447 Altering the active sites of essential proteins in cell division is risky and requires a delicate
448 balance between antibiotic avoidance and fitness loss. Accumulation of sufficient mutations
449 in the appropriate order is aided both by the simultaneous recombination of multiple donor
450 fragments distally around the genome, and by the occurrence of complex non-contiguous
451 events. The experimental transformation experiments combined with whole genome
452 sequencing as performed here provide valuable insights into viable and non-viable
453 evolutionary paths toward AMX resistance development in the pneumococcus. The strong
454 co-dependence among different proteins and their alleles creates significant challenges for
455 complete understanding of resistance mechanisms, and emphasizes the importance of
456 combining data from phenotypic, molecular, genomic, and genome-wide association studies.
457

458 # Methods

459 ***Bacterial strains, growth conditions, and antibiotics***

460 *S. pneumoniae* strains are shown in Table 1 and Table S1. Bacteria were cultured in liquid C+Y
461 medium with no shaking at 37°C. C+Y media was adapted from Adams and Roe (Martin et al.,
462 1995).

463 For transformation, *S. pneumoniae* was grown in C+Y (pH 6.8) at 37°C to OD_{595} 0.1.
464 Competence was induced by addition of 100 ng/ml synthetic CSP-1 (D39V) or CSP-2 (TIGR4)
465 and 12 min incubation at 37°C. DNA uptake occurred during 20 min at 30°C, followed by
466 dilution and recovery for 1.5 hr. Transformants were selected by plating inside Columbia agar
467 supplemented with 3% defibrinated sheep blood (CBA, Thermo Scientific) containing the
468 appropriate antibiotic and incubated at 37°C in 5% CO_2 overnight. Successful transformants
469 were confirmed by PCR and Sanger sequencing (Microsynth).

470 Strains were stocked at OD_{595} 0.3 in C + Y with 15% glycerol at -80°C.

471 AMX (Sigma Aldrich) powder was dissolved initially in 100% DMSO. This solution was diluted
472 in molecular grade water with 4% DMSO to two concentrations, 100 µg/mL and 1 mg/mL, and
473 stored at -80°C.

474

475

Table 1: Key strains used in this study. The full collection of recombinant strains and their AMX MIC can be found in Table S1

Strain Name	Strain ID	Genotype and relevant characteristics	AMX MIC (µg/mL)	reference
D39V	VL1	Serotype 2 laboratory strain, AMX-S	0.001	Slager et al., 2018
TIGR4	VL2177	Serotype 4 laboratory strain, AMX-S	0.016	Tettelin et al., 2001
11A	SN75752 VL1313	Serotype 11A ST6521 clinical isolate, AMX-R	4	German National Reference Center for Streptococci
AMR37	VL4481	D39V; recombinant strain, generation 1	0.094	This study
AMR38	VL4482	D39V; recombinant strain, generation 1	0.094	This study
AMR53	VL3196	D39V; recombinant strain, generation 2	2	This study
AMR95	VL4484	D39V; recombinant strain, generation 2	1.5	This study
EB31	VL4495	TIGR4; recombinant strain, generation 2	4	This study
D39V^{2x37}	VL4496	D39V; *pbp2x37*	0.023	This study
D39V^{2x38}	VL4302	D39V; *pbp2x38*	0.064	This study
D39V^{2b37}	VL4497	D39V; *pbp2b37*	0.023	This study
D39V^{2b38}	VL4498	D39V; *pbp2b38*	0.023	This study
D39V$^{2x37\text{-}2b37}$	VL4499	D39V; *pbp2x37*; *pbp2b37*	0.094	This study
D39V$^{2x38\text{-}2b38}$	VL3895	D39V; *pbp2x38*; *pbp2b38*	0.094	This study
D39V^{M53}	VL3960	D39V; *murM53*	0.023	This study
D39V^{1a53}	VL4159	D39V; *pbp1a53*	0.016	This study
D39V^{1a95}	VL4160	D39V; *pbp1a95*	0.016	This study
D39V$^{2x38\text{-}2b38\text{-}M53}$	VL3961	D39V; *pbp2x38*; *pbp2b38*; *murM53*	0.38	This study
D39V$^{2x38\text{-}2b38\text{-}M95}$	VL3962	D39V; *pbp2x38*; *pbp2b38*; *murM95*	0.5	This study
D39V$^{2x38\text{-}2b38\text{-}1a53}$	VL3896	D39V; *pbp2x38*; *pbp2b38*; *pbp1a53*	0.75	This study
D39V$^{2x38\text{-}2b38\text{-}M53\text{-}1a53}$	VL3963	D39V; *pbp2x38*; *pbp2b38*; *murM53*; *pbp1a53*	2	This study
D39V$^{2x38\text{-}2b38\text{-}M95\text{-}1a95}$	VL4500	D39V; *pbp2x38*; *pbp2b38*; *murM95*; *pbp1a95*	1.5	This study
AMR53^{2b31}	VL4174	AMR53; *pbp2b31*	6	This study
AMR95^{2b31}	VL4184	AMR95; *pbp2b31*	6	This study

476

477 ***Minimum Inhibitory Concentrations (MICs)***

478 Bacteria were grown in C+Y broth to OD_{595} 0.1, then AMX MIC was determined using E-tests
479 (Biomeriaux, Lyon) on Mueller Hinton agar containing 5% defibrinated sheep's blood. MICs
480 were read after 18 h incubation at 37°C and 5% CO_2.

481 Strains with MICs below the limit of the E-tests (0.016 µg/mL) were tested in Mueller Hinton
482 cation-adjusted broth with 5% defibrinated sheep's blood using the broth micro-dilution
483 method (Charles et al., 2016). Briefly, bacteria were streaked onto MH2-blood plates and
484 grown overnight. Colonies were picked from plates and ressupended in PBS (pH 7.4) to
485 McFarlane standard 0.5. This inoculum was diluted 100-fold into 96-well plates containing
486 MH2-blood broth and AMX (in 2-fold concentration steps) then plated on agar plates as a
487 control for contamination and cell density. Plates were incubated for 18 hours at 37°C and 5%
488 CO_2. MIC was defined as the lowest concentration of antibiotic with less than 10% visible
489 growth.

490

491 ***Growth curves and analysis***

492 Strains were precultured in C+Y broth to OD 0.1, then diluted 100-fold into 96-well microtiter
493 plates, containing fresh C+Y and AMX. The OD_{595} was measured every 10 min for 12 hr in a
494 plate reader (Infinite F200, Tecan) with incubation at 37°C. All strains were tested in triplicate
495 Area under the curve was determined using TecanExtracter (Dénéréaz, unpublished). The
496 AUC of each replicate was divided by that of the no antibiotic control for each strain, to
497 normalize for strain-dependent differences in growth. The mean and standard error of the
498 mean (SEM) of the normalized AUC was determined for three biological replicates.

499 Statistical significance of maximum specific growth rate (µ/h) was determined using one-way
500 ANOVA with a Tukey correction for multiple testing.

501

502 ***Bocillin-FL binding assay***

503 Bocillin-FL is a fluorescently labelled penicillin molecule which can be used to visualise and
504 quantify PBP-penicillin binding affinity *in vitro*. Strains were grown to OD 0.2 in 4 mL C+Y,
505 washed and resuspended in phosphate buffered saline (PBS), then incubated for 30 min at
506 37C in 5 µg/mL bocillin-FL (Invitrogen). Cells were washed in ice cold PBS, then lysed by
507 sonication (10 x 1s pulses at 30% power). The cell lysate was spun down and supernatant
508 removed to collect the membrane fraction, which was homogenized by sonication (1s pulse

509 at 10%). Total protein concentration was determined by nanodrop, then samples were diluted
510 in NuPAGE LDS sample buffer (Life Technologies) with 10 mM DTT and incubated at 95°C for
511 5 min. Samples were loaded into two 15-well Novex™ WedgeWell™ 10% Tris-Glycine 1.0 mm
512 Mini Protein Gels (Invitrogen), to a total protein amount of approximately 1.8 mg in a
513 maximum volume of 30 µL. Where necessary, gels were imaged simultaneously on an
514 Amersham Typhoon (GE Healthcare) with Cy2 DIGE filter setup. Bands were quantified using
515 ImageQuant (GE Healthcare). As all strains tested had identical PBP3 proteins, the intensities
516 of the PBP1a/b, PBP2x/a, and PBP2b bands were divided by the PBP3 band intensity of the
517 corresponding sample for normalisation. Imaging and quantification were performed in
518 duplicate. Coomassie Blue staining was also performed, to confirm equal sample loading.
519
520 ***Phase-contrast time-lapse microscopy***
521 For time-lapse microscopy, cells were pre-cultured in liquid C + Y medium at 37°C and spotted
522 on a low-melting 1.2% C + Y agarose patch, with or without AMX at 1 µg/mL. Phase-contrast
523 pictures were taken every 10 min as described (de Jong et al., 2011) using a Leica DMi8 with
524 a 100x phase contrast objective.
525
526 ***Isolation of genomic DNA***
527 10 mL of OD_{595} 0.2 culture was pelleted by centrifugation, then resuspended in Nuclei Lysis
528 solution (Promega) supplemented with 0.05% SDS, 0.025% deoxycholate (DOC), and 200
529 µg/mL RNase A. This was incubated at 37°C for 20 minutes, 80°C for 5 minutes, then 37°C for
530 10 minutes. Protein Precipitation Solution (Promega) was added to the lysate, vortexed
531 vigorously, then incubated on ice for 10 minutes. The precipitated protein was pelleted by
532 centrifugation and the supernatant transferred into isopropanol to precipitate the DNA,
533 which was then collected by centrifugation. DNA was washed once in 70% ethanol before air
534 drying and resuspension in the appropriate buffer (either TE buffer or molecular grade water).
535 DNA was run on a 1% agarose gel to confirm no significant degradation had occurred, and
536 stored at 4°C.
537
538 ***Serial Transformation of* S. pneumoniae *with genomic DNA***
539 AMX susceptible recipient strains were transformed with 100 µg/mL genomic DNA isolated
540 from AMX resistant strain 11A (Table 1) as above, with the following modifications. DNA

541 uptake occurred during 30 min, followed by recovery for 2 hrs. Transformants were selected
542 by plating inside Columbia agar supplemented with 5% defibrinated sheep blood and AMX
543 (0.03 µg/mL). Ten colonies were then streaked onto CBA plates containing AMX. The next
544 day, single colonies were grown up in C+Y with AMX and stocked. MICs were determined for
545 these 10 strains, which were then subjected to another round of transformation and selection
546 on a range of AMX concentrations (0.17 - 0.5 µg/mL), and 5-10 single colonies were picked
547 for each of the 10 strains transformed. These were isolated, and MICs determined, as above.
548 To test for significant differences between MICs of second-generation strains in different
549 lineages, a Fisher's Exact Test with Monte Carlo p-value simulation was used.
550 To control for spontaneous mutations arising during transformation and recombination, cells
551 transformed with either no DNA, or with D39V genomic DNA, were also plated in CBA with
552 AMX (0.03). Neither resulted in visible colonies.

553

554 ***Whole genome sequencing and quality control***

555 Genomic DNA from recombinant strains from each recipient background, as well as 11A and
556 TIGR4 were Illumina sequenced (PE150, Novogene and Eurofins Genomics), with a mean
557 coverage of 600-fold. Reads were trimmed using Trimmomatic (Bolger et al., 2014), then
558 assembled using SPAdes (Nurk et al., 2013). Assembly quality was assessed with Quast
559 (Gurevich et al., 2013), and read depth was determined in samtools (Li et al., 2009). Previously
560 published D39V Illumina reads were filtered as above and used where necessary (GEO
561 accessions GSE54199 and GSE69729) (Slager et al., 2014). Allelic exchange strains ($D39V^{M53}$,
562 $D39V^{2x38\text{-}2b38\text{-}M53\text{-}1a53}$, $D39V^{1a53}$, $D39V^{2x38\text{-}2b38\text{-}M95\text{-}1a95}$) were treated in the same way, then
563 variants were called using bbmap (Bushnell, 2013), Freebayes (Garrison and Marth, 2012),
564 and vcftools (Danecek et al., 2011), in order to check for random mutations arising elsewhere
565 in the genome.
566 11A, TIGR4, and a subset of recombinant strains were sent for PacBio sequencing (Sequel I
567 and II, Lausanne Genomic Technologies Facility). Demultiplexing and quality control were
568 performed using SMRTlink (PacBio), then reads shorter than 1000 bp were removed with
569 filtlong (Wick, 2017). Recombinant strain reads were mapped to the recipient reference
570 genome using NGMLR and structural variants (SVs) called with sniffles with default settings,
571 except with read mapping quality > 40 and read depth > 50 (Sedlazeck et al., 2018). Imprecise

572 SVs were then filtered out. DNA methylation detection was performed using motifMaker
573 (Clark et al., 2012).
574 Raw read files are deposited with NCBI Sequence Read Archive under BioProject
575 PRJNA789167 (Individual SRA accession numbers for recombinant strains can be found in
576 Table S4).
577
578 ***Hybrid assemblies of reference genomes***
579 As PacBio sequencing depth was greater than 200x, genomes were assembled in a long-read
580 only manner using Trycycler (Wick et al., 2021), followed by short-read polishing.
581 Briefly, filtered reads were subsampled 12 times and *de novo* assembled in four different
582 assemblers, flye (Kolmogorov et al., 2019), raven (Wang et al., 2018), wtdbg2 (Ruan and Li,
583 2020), and miniasm plus minipolish (Li, 2018, 2016). Some assemblies were removed during
584 the Trycycler cluster and reconcile steps, leaving the final consensus sequence to be built
585 from seven to eight assemblies. The consensus assembly was subjected to rounds of polishing
586 with PacBio reads using pbmm2 and pbgcpp (PacBio Toolkit), followed by one round of short-
587 read polishing with Pilon (Walker et al., 2014).
588 Genomes were annotated in Prokka (Seemann, 2014) using Barrnap and Aragorn (Laslett and
589 Canback, 2004; Seemann, 2019) and are deposited at NCBI under BioProject PRJNA789167
590 (accession numbers currently in process).
591
592 ***Recombination detection with NGS***
593 Competitive mapping of filtered illumina reads onto a pseudogenome containing both
594 recipient and donor chromosomes was used for crude visualization of recombination loci
595 (bbmap) (Matthey et al., 2019). In order to characterize these loci more accurately, filtered
596 reads of recombinant and recipient strains were mapped onto the 11A hybrid genome
597 assembly using smalt, then variants were called with bcftools (Li, 2011). SNPs were filtered as
598 described previously (Cowley et al. 2018), and used to build a consensus alignment of donor,
599 recipient, and recombinant strains. The consensus alignment was run through a python script
600 designed to identify SNPs between recombinant and donor which are not shared with the
601 recipient genome. Once identified, the match was extended until the donor and recombinant
602 sequences are no longer identical, then the start, end, and length of detected recombination
603 events are extracted (Cowley et al 2018).

604

605 ***Identifying non-contiguous recombination events***

606 Many recombination events were located very close together, with sometimes only a few
607 recipient allele SNPs separating the two, suggesting a single donor DNA molecule as the
608 source. To determine if events were significantly close together, a bootstrapping approach
609 was applied (Croucher et al., 2012). Firstly, the distances between one recombination event
610 and each of the other recombination events in a single genome were calculated. The circular
611 chromosome gives two values, and the shortest distance between any two events was added
612 to the test population. This was calculated for every sequenced strain in the D39V and TIGR4
613 recombinants, and for second-generation strains any prior events carried through from the
614 first-generation were removed from the dataset. The shortest recombination distance within
615 a strain became the test value (d_{test}), and then the test population was sampled (with
616 replacement).

617 The distribution of a bootstrapped sample (same size as the test population) was used to test
618 the hypothesis that d_{test} was significantly shorter than expected under the null hypothesis
619 that recombination events are located at random around the chromosome. A Holm
620 correction was applied to account for multiple testing, based on the number of recombination
621 events in the strain. Bootstrap tests were performed one thousand times for each d_{test} value
622 and considered significantly short if the null hypothesis was rejected at least 95% of the time.
623 If a d_{test} value was significant, then the distance between the next shortest pairing within the
624 strain became d_{test}, and was tested in the same fashion. This continued until a d_{test} where the
625 null hypothesis could not be rejected.

626 When recombination events were considered significantly close together, they were linked
627 together into non-contiguous recombination events.

628

629 ***Confirming the origins of non-contiguous recombination events in vivo***

630 A 4.25 Kb region of the 11A genome spanning *pbp2x* was used to test the origin of non-
631 contiguous recombination. This region included an 846 bp stretch with SNPs conferring a
632 small decrease in AMX susceptibility sufficient for selection. One long fragment spanning the
633 entire region was amplified with OVL5375 and OVL5378. Two shorter fragments were then
634 amplified, an upstream fragment (Up) with OVL5379 and OVL5375 (2.84 Kb) and a
635 downstream fragment (Down) with OVL5376 and OVL5378 (2.26 Kb), which overlapped at

636 the SNPs determined to be necessary for selection (Table S2, S5). The three donor DNA
637 templates used in the experiment and their SNPs are shown in Figure 6C (Table S6).
638 D39V was transformed as above, with equimolar quantities of each fragment separately, as
639 well as a combination of the two short fragments, and a negative control with no DNA.
640 Transformants were selected on AMX (0.015 µg/mL), and the transformation efficiency was
641 determined by dividing by the total viable count. Individual colonies were restreaked on AMX,
642 then single colonies were picked and the 4.25 Kb region of interest was amplified and Sanger
643 sequenced (Microsynth, Supp. Table ## oligos). Nucleotide sequences were aligned in Mega
644 (Kumar et al., 2018).
645 As molecule length affects transformation efficiency (Keller et al., 2019; Kurushima et al.,
646 2020; Lee et al., 1998), an additional experiment was performed, where the amplified
647 fragments were all extended to 6 Kb by the addition of non-homologous DNA amplified from
648 *E. coli* and ligated to one end using Golden Gate assembly with BsmBI and T4 DNA ligase (NEB,
649 Vazyme). All oligos and the corresponding templates used in the cloning for these
650 experiments are outlined in Table S6, and a comprehensive oligo list can be found in Table S2.
651 The assemblies were then amplified to ensure high quality of transforming fragments,
652 resulting in three fragments of equal size, with differing lengths of homologous regions to the
653 *pbp2x* locus. These were then transformed, amplified, and Sanger sequenced as above, and
654 the transformation efficiency determined.
655
656 ***Gene and protein alignments***
657 Nucleotide sequences of *pbp* and *murM* genes were translated using Emboss:TransSeq
658 (Madeira et al., 2019). Alignments were performed with Muscle (Edgar, 2004). Phylogenetic
659 trees were produced using concatenated protein alignments of Pbp2x, Pbp2b, Pbp1a, and
660 MurM as input for FastTree (default settings), and visualised in ITOL (Letunic and Bork, 2021;
661 Price et al., 2009).
662
663 ***Amplification and transformation of* pbp *and* murM *loci for allelic exchange experiments***
664 Genes for *pbps* were amplified with Phanta Max Super-Fidelity DNA Polymerase (Vazyme)
665 and primers ordered from Sigma (Table S2). Equimolar quantities of PCR products were used
666 for transformation. To avoid transforming mutations in *murN* alongside those in *murM*, alleles
667 at this locus were cloned into a construct with D39V flanking sequences. The upstream and

668 downstream fragments were amplified from D39V with OVL5540/OVL5779 and
669 OVL5780/OVL5541 respectively, and the *murM* allele from AMR53 or AMR95 with
670 OVL5777/OVL5778. Fragments were then assembled using BsmBI and T4 DNA ligase.
671 *pbp2x* and *pbp2b* alleles from AMR37 and AMR38 were transformed into D39V as above,
672 selected on 0.012 µg/mL, 0.015 µg/mL, 0.02 µg/mL AMX, and confirmed by Sanger
673 sequencing. D39V$^{2x38-2b38}$ (Table 1) was then used as the recipient for *murM* and *pbp1a* alleles
674 from AMR53 and AMR95, with selection on 0.2 µg/mL, 0.5 µg/mL and 1 µg/mL AMX.
675

676 **Acknowledgements**

677 We would like to thank Mark van der Linden at the German National Reference Center for
678 Streptococci for the 11A (SN75752) clinical isolate, and the Lausanne Genomic Technologies
679 Facility for their valuable work in PacBio sequencing and data quality control. We would also
680 like to thank Laetitia Attaiech, Nicholas Croucher, Arnau Domenech, Alice Wallef, Vincent de
681 Bakker, Julien Dénéréaz, and the rest of the Veening Lab for their help, contributions, and
682 feedback. P.G. was supported by the University of Lausanne Faculty of Biology and Medicine
683 PhD fellowship. Work in the Veening lab is supported by the Swiss National Science
684 Foundation (SNSF) (project grant 310030_192517), SNSF JPIAMR grant (40AR40_185533),
685 SNSF NCCR 'AntiResist' (51NF40_180541) and ERC consolidator grant 771534-
686 PneumoCaTChER.
687

688 **References**

689 Albarracín Orio AG, Piñas GE, Cortes PR, Cian MB, Echenique J. 2011. Compensatory evolution of *pbp* mutations
690 restores the fitness cost imposed by β-lactam resistance in *Streptococcus pneumoniae*. *PLoS Pathogens*
691 **7**:e1002000. doi:10.1371/journal.ppat.1002000

692 Alloing G, Martin B, Granadel C, Claverys JP. 1998. Development of competence in *Streptococcus pneumoniae*:
693 Pheromone autoinduction and control of quorum sensing by the oligopeptide permease. *Molecular*
694 *Microbiology* **29**:75–83. doi:10.1046/J.1365-2958.1998.00904.X

695 Arnold BJ, Gutmann MU, Grad YH, Sheppard SK, Corander J, Lipsitch M, Hanage WP. 2018. Weak epistasis may
696 drive adaptation in recombining bacteria. *Genetics* **208**:1247–1260. doi:10.1534/genetics.117.300662

697 Attaiech L, Olivier A, Mortier-Barrière I, Soulet AL, Granadel C, Martin B, Polard P, Claverys JP. 2011. Role of the
698 single-stranded dna-binding protein Ssbb in pneumococcal transformation: Maintenance of a reservoir for
699 genetic plasticity. *PLoS Genetics* **7**:e1002156. doi:10.1371/journal.pgen.1002156

700 Bell JC, Kowalczykowski SC. 2016. RecA: Regulation and Mechanism of a Molecular Search Engine. *Trends in*
701 *Biochemical Sciences*. doi:10.1016/j.tibs.2016.04.002

Berg KH, Stamsås GA, Straume D, Håvarstein LS. 2013. Effects of low PBP2b levels on cell morphology and peptidoglycan composition in *Streptococcus pneumoniae* R6. *Journal of bacteriology* **195**:4342–4354. doi:10.1128/JB.00184-13

Bergé MJ, Kamgoué A, Martin B, Polard P, Campo N, Claverys J-P. 2013. Midcell Recruitment of the DNA Uptake and Virulence Nuclease, EndA, for Pneumococcal Transformation. *PLOS Pathogens* **9**:e1003596. doi:10.1371/JOURNAL.PPAT.1003596

Bolger AM, Lohse M, Usadel B. 2014. Trimmomatic: a flexible trimmer for Illumina sequence data. *Bioinformatics (Oxford, England)* **30**:2114–20. doi:10.1093/bioinformatics/btu170

Bushnell B. 2013. BBMap download | SourceForge.net. *SourceForge*. https://sourceforge.net/projects/bbmap/

Cafini F, del Campo R, Alou L, Sevillano D, Morosini MI, Baquero F, Prieto J, García E, Casal J, Fenoll A, de la Campa AG, Bouza E, Baquero F, Soriano F, Pallarés R, Liñares J, Garau J, Lacasa JM, Latorre C, Pérez-Trallero E, García de Lomas J, Fleites A. 2006. Alterations of the penicillin-binding proteins and *murM* alleles of clinical *Streptococcus pneumoniae* isolates with high-level resistance to amoxicillin in Spain. *Journal of Antimicrobial Chemotherapy* **57**:224–229. doi:10.1093/jac/dki442

Càmara J, Cubero M, Martín-Galiano AJ, García E, Grau I, Nielsen JB, Worning P, Tubau F, Pallarés R, Domínguez MÁ, Kilian M, Liñares J, Westh H, Ardanuy C. 2018. Evolution of the β-lactam-resistant *Streptococcus pneumoniae* PMEN3 clone over a 30 year period in Barcelona, Spain. *Journal of Antimicrobial Chemotherapy* **73**:2941–2951. doi:10.1093/jac/dky305

Charles MK, Berenger BM, Turnbull L, Rennie R, Fuller J. 2016. Variability of β-lactam susceptibility testing for *Streptococcus pneumoniae* using 4 commercial test methods and broth microdilution. *Diagnostic Microbiology and Infectious Disease* **84**:240–245. doi:10.1016/J.DIAGMICROBIO.2015.11.014

Chesnel L, Carapito R, Croizé J, Dideberg O, Vernet T, Zapun A. 2005. Identical penicillin-binding domains in penicillin-binding proteins of *Streptococcus pneumoniae* clinical isolates with different levels of beta-lactam resistance. *Antimicrobial agents and chemotherapy* **49**:2895–2902. doi:10.1128/AAC.49.7.2895

Chewapreecha C, Harris SR, Croucher NJ, Turner C, Marttinen P, Cheng L, Pessia A, Aanensen DM, Mather AE, Page AJ, Salter SJ, Harris D, Nosten F, Goldblatt D, Corander J, Parkhill J, Turner P, Bentley SD. 2014. Dense genomic sampling identifies highways of pneumococcal recombination. *Nature Genetics* **46**:305–309. doi:10.1038/ng.2895

Clark TA, Murray IA, Morgan RD, Kislyuk AO, Spittle KE, Boitano M, Fomenkov A, Roberts RJ, Korlach J. 2012. Characterization of DNA methyltransferase specificities using single-molecule, real-time DNA sequencing. *Nucleic Acids Research* **40**. doi:10.1093/nar/gkr1146

Claverys JP, Lacks SA. 1986. Heteroduplex deoxyribonucleic acid base mismatch repair in bacteria. *Microbiological Reviews*. doi:10.1128/mmbr.50.2.133-165.1986

Cowley LA, Petersen FC, Junges R, Jimson D. Jimenez M, Morrison DA, Hanage WP. 2018. Evolution via recombination: Cell-to-cell contact facilitates larger recombination events in *Streptococcus pneumoniae*. *PLOS Genetics* **14**:e1007410. doi:10.1371/journal.pgen.1007410

Croucher NJ, Harris SR, Barquist L, Parkhill J, Bentley SD. 2012. A high-resolution view of genome-wide pneumococcal transformation. *PLoS Pathogens* **8**:e1002745. doi:10.1371/journal.ppat.1002745

Croucher NJ, Harris SR, Fraser C, Quail MA, Burton J, van der Linden M, McGee L, von Gottberg A, Song JH, Ko KS, Pichon B, Baker S, Parry CM, Lambertsen LM, Shahinas D, Pillai DR, Mitchell TJ, Dougan G, Tomasz A, Klugman KP, Parkhill J, Hanage WP, Bentley SD. 2011. Rapid pneumococcal evolution in response to clinical interventions. *Science* **331**:430–434. doi:10.1126/SCIENCE.1198545

Danecek P, Auton A, Abecasis G, Albers CA, Banks E, DePristo MA, Handsaker RE, Lunter G, Marth GT, Sherry ST, McVean G, Durbin R. 2011. The variant call format and VCFtools. *Bioinformatics* **27**:2156–2158. doi:10.1093/bioinformatics/btr330

747 Danilowicz C, Yang D, Kelley C, Prévost C, Prévost P, Prentiss M. 2015. The poor homology stringency in the
748 heteroduplex allows strand exchange to incorporate desirable mismatches without sacrificing recognition
749 in vivo. *Nucleic Acids Research* **43**:6473–6485. doi:10.1093/nar/gkv610

750 Demerec M. 1945. Production of Staphylococcus strains resistant to various concentrations of penicillin.
751 *Proceedings of the National Academy of Sciences* **31**:16–24.

752 Desai B v, Morrison DA. 2007. Transformation in *Streptococcus pneumoniae*: Formation of eclipse complex in a
753 *coiA* mutant implicates CoiA in genetic recombination. *Molecular Microbiology* **63**:1107–1117.
754 doi:10.1111/j.1365-2958.2006.05558.x

755 Doern G v, Brueggemann A, Holley HP, Rauch AM. 1996. Antimicrobial resistance of *Streptococcus pneumoniae*
756 recovered from outpatients in the United States during the winter months of 1994 to 1995: results of a
757 30-center national surveillance study. *Antimicrobial agents and chemotherapy* **40**:1208–13.
758 doi:10.1128/AAC.40.5.1208

759 Doit C, Loukil C, Fitoussi F, Geslin P, Bingen E. 1999. Emergence in France of Multiple Clones of Clinical
760 *Streptococcus pneumoniae* Isolates with High-Level Resistance to Amoxicillin. *Antimicrobial Agents and*
761 *Chemotherapy* **43**:1480–1483. doi:10.1128/AAC.43.6.1480

762 Donati C, Hiller NL, Tettelin H, Muzzi A, Croucher NJ, Angiuoli S v., Oggioni M, Dunning Hotopp JC, Hu FZ, Riley
763 DR, Covacci A, Mitchell TJ, Bentley SD, Kilian M, Ehrlich GD, Rappuoli R, Moxon ER, Masignani V. 2010.
764 Structure and dynamics of the pan-genome of *Streptococcus pneumoniae* and closely related species.
765 *Genome Biology* **11**:R107. doi:10.1186/gb-2010-11-10-r107

766 Dowson CG, Coffey TJ, Kell C, Whiley RA. 1993. Evolution of penicillin resistance in *Streptococcus pneumoniae*;
767 the role of *Streptococcus mitis* in the formation of a low affinity PBP2B in *S. pneumoniae*. *Molecular*
768 *Microbiology* **9**:635–643. doi:10.1111/j.1365-2958.1993.tb01723.x

769 du Plessis M, Bingen E, Klugman KP, Plessis M du, Bingen E, Klugman KP, du Plessis M, Bingen E, Klugman KP.
770 2002. Analysis of Penicillin-Binding Protein Genes of Clinical Isolates of *Streptococcus pneumoniae* with
771 Reduced Susceptibility to Amoxicillin. *Antimicrobial Agents and Chemotherapy* **46**:2349–2357.
772 doi:10.1128/AAC.46.8.2349

773 Edgar RC. 2004. MUSCLE: Multiple sequence alignment with high accuracy and high throughput. *Nucleic Acids*
774 *Research* **32**:1792–1797. doi:10.1093/nar/gkh340

775 el Khoury JY, Boucher N, Bergeron MG, Leprohon P, Ouellette M. 2017. Penicillin induces alterations in glutamine
776 metabolism in *Streptococcus pneumoniae*. *Scientific Reports* **7**. doi:10.1038/s41598-017-15035-y

777 Feng Z, Li J, Zhang JR, Zhang X. 2014. Qdnamod: A statistical model-based tool to reveal intercellular
778 heterogeneity of DNA modification from SMRT sequencing data. *Nucleic Acids Research* **42**:13488–13499.
779 doi:10.1093/nar/gku1097

780 Figueiredo TA, Sobral RG, Ludovice AM, de Almeida JMF, Bui NK, Vollmer W, de Lencastre H, Tomasz A. 2012.
781 Identification of Genetic Determinants and Enzymes Involved with the Amidation of Glutamic Acid
782 Residues in the Peptidoglycan of *Staphylococcus aureus*. *PLOS Pathogens* **8**:e1002508.
783 doi:10.1371/JOURNAL.PPAT.1002508

784 Filipe SR, Severina E, Tomasz A. 2002. The *murMN* operon: A functional link between antibiotic resistance and
785 antibiotic tolerance in *Streptococcus pneumoniae*. *Proceedings of the National Academy of Sciences*
786 **99**:1550–1555. doi:10.1073/PNAS.032671699

787 Filipe SR, Tomasz A. 2000. Inhibition of the expression of penicillin resistance in *Streptococcus pneumoniae* by
788 inactivation of cell wall muropeptide branching genes. *Proceedings of the National Academy of Sciences*
789 **97**:4891–4896. doi:https://doi.org/10.1073/pnas.080067697

790 Forget AL, Kowalczykowski SC. 2012. Single-molecule imaging of DNA pairing by RecA reveals a three-
791 dimensional homology search. *Nature 2012 482:7385* **482**:423–427. doi:10.1038/nature10782

792 Garcia-Bustos J, Tomasz A. 1990. A biological price of antibiotic resistance: major changes in the peptidoglycan
793 structure of penicillin-resistant pneumococci. *Proceedings of the National Academy of Sciences of the*
794 *United States of America* **87**:5415–9. doi:10.1073/pnas.87.14.5415

795 Garrison E, Marth G. 2012. Haplotype-based variant detection from short-read sequencing. *arXiv.org*.

796 Gasc AM, Sicard AM, Claverys JP. 1989. Repair of single- and multiple-substitution mismatches during
797 recombination in *Streptococcus pneumoniae*. *Genetics* **121**:29–36. doi:10.1093/genetics/121.1.29

798 Grebe T, Paik J, Hakenbeck R. 1997. A novel resistance mechanism against β-lactams in *Streptococcus*
799 *pneumoniae* involves CpoA, a putative glycosyltransferase. *Journal of Bacteriology* **179**:3342–3349.
800 doi:10.1128/jb.179.10.3342-3349.1997

801 Guenzi E, Gasc A-M, Sicard MA, Hakenbeck R. 1994. A two-component signal-transducing system is involved in
802 competence and penicillin susceptibility in laboratory mutants of *Streptococcus pneumoniae*. *Molecular*
803 *Microbiology* **12**:505–515. doi:10.1111/j.1365-2958.1994.tb01038.x

804 Gurevich A, Saveliev V, Vyahhi N, Tesler G. 2013. QUAST: quality assessment tool for genome assemblies.
805 *Bioinformatics* **29**:1072–1075. doi:10.1093/bioinformatics/btt086

806 Gurney T, Fox MS. 1968. Physical and genetic hybrids formed in bacterial transformation. *Journal of Molecular*
807 *Biology* **32**:83–100. doi:10.1016/0022-2836(68)90147-2

808 Hakenbeck R, Brückner R, Denapaite D, Maurer P. 2012. Molecular mechanisms of β-lactam resistance in
809 *Streptococcus pneumoniae*. *Future Microbiology*. doi:10.2217/fmb.12.2

810 Hakenbeck R, Nig AK, Kern I, van der Linden M, Keck W, Billot-Klein D, Legrand R, Schoot B, Gutmann L. 1998.
811 Acquisition of Five High-M r Penicillin-Binding Protein Variants during Transfer of High-Level beta-Lactam
812 Resistance from *Streptococcus mitis* to *Streptococcus pneumoniae*. *Journal of Bacteriology* **180**:1831–
813 1840.

814 Hiller NL, Ahmed A, Powell E, Martin DP, Eutsey R, Earl J, Janto B, Boissy RJ, Hogg J, Barbadora K, Sampath R,
815 Lonergan S, Post JC, Hu FZ, Ehrlich GD. 2010. Generation of Genic Diversity among *Streptococcus*
816 *pneumoniae* Strains via Horizontal Gene Transfer during a Chronic Polyclonal Pediatric Infection. *PLOS*
817 *Pathogens* **6**:e1001108. doi:10.1371/JOURNAL.PPAT.1001108

818 Hotchkiss RD. 1951. Transfer of penicillin resistance in pneumococci by the desoxyribonucleate derived from
819 resistant cultures. *Cold Spring Harbor symposia on quantitative biology* **16**:457–461.
820 doi:10.1101/SQB.1951.016.01.032

821 Hsieh P, Camerini-Otero CS, Camerini-Otero RD. 1992. The synapsis event in the homologous pairing of DNAs:
822 RecA recognizes and pairs less than one helical repeat of DNA. *Proceedings of the National Academy of*
823 *Sciences of the United States of America* **89**:6492–6496. doi:10.1073/pnas.89.14.6492

824 Humbert O, Prudhomme M, Hakenbeck R, Dowson CG, Claverys JP. 1995. Homeologous recombination and
825 mismatch repair during transformation in *Streptococcus pneumoniae*: Saturation of the Hex mismatch
826 repair system. *Proceedings of the National Academy of Sciences of the United States of America* **92**:9052–
827 9056. doi:10.1073/pnas.92.20.9052

828 Kalizang'oma A, Chaguza C, Gori A, Davison C, Beleza S, Antonio M, Beall B, Goldblatt D, Kwambana-Adams B,
829 Bentley SD, Heyderman RS. 2021. *Streptococcus pneumoniae* serotypes that frequently colonise the
830 human nasopharynx are common recipients of penicillin-binding protein gene fragments from
831 *Streptococcus mitis*. *Microbial Genomics* **7**:000622. doi:10.1099/mgen.0.000622

832 Keller LE, Rueff A-S, Kurushima J, Veening J-W. 2019. Three new integration vectors and fluorescent proteins for
833 use in the opportunistic human pathogen *Streptococcus pneumoniae*. *Genes* **10**:394.
834 doi:10.3390/genes10050394

835 Kocaoglu O, Tsui H-CT, Winkler ME, Carlson EE. 2015. Profiling of β-lactam selectivity for penicillin-binding
836 proteins in *Streptococcus pneumoniae* D39. *Antimicrobial Agents and Chemotherapy* **59**:3548–3555.
837 doi:10.1128/AAC.05142-14

838 Kolmogorov M, Yuan J, Lin Y, Pevzner PA. 2019. Assembly of long, error-prone reads using repeat graphs. *Nature*
839 *Biotechnology* **37**:540–546. doi:10.1038/s41587-019-0072-8

840 Kosowska K, Jacobs MR, Bajaksouzian S, Koeth L, Appelbaum PC. 2004. Alterations of Penicillin-Binding Proteins
841 1A, 2X, and 2B in *Streptococcus pneumoniae* Isolates for Which Amoxicillin MICs Are Higher than Penicillin
842 MICs **48**. doi:10.1128/AAC.48.10.4020-4022.2004

843 Kumar S, Stecher G, Li M, Knyaz C, Tamura K. 2018. MEGA X: Molecular evolutionary genetics analysis across
844 computing platforms. *Molecular Biology and Evolution* **35**:1547–1549. doi:10.1093/molbev/msy096

845 Kurushima J, Campo N, van Raaphorst R, Cerckel G, Polard P, Veening JW. 2020. Unbiased homeologous
846 recombination during pneumococcal transformation allows for multiple chromosomal integration events.
847 *eLife* **9**:1–70. doi:10.7554/ELIFE.58771

848 Lacks S, Greenberg B. 1976. Single-strand breakage on binding of DNA to cells in the genetic transformation of
849 Diplococcus pneumoniae. *Journal of Molecular Biology* **101**:255–275. doi:10.1016/0022-2836(76)90376-4

850 Lacks S, Neuberger M. 1975. Membrane location of a deoxyribonuclease implicated in the genetic
851 transformation of Diplococcus pneumoniae. *Journal of Bacteriology* **124**:1321–1329.
852 doi:10.1128/jb.124.3.1321-1329.1975

853 Laslett D, Canback B. 2004. ARAGORN, a program to detect tRNA genes and tmRNA genes in nucleotide
854 sequences. *Nucleic Acids Research* **32**:11–16. doi:10.1093/nar/gkh152

855 Laurenceau R, Péhau-Arnaudet G, Baconnais S, Gault J, Malosse C, Dujeancourt A, Campo N, Chamot-Rooke J, le
856 Cam E, Claverys JP, Fronzes R. 2013. A Type IV Pilus Mediates DNA Binding during Natural Transformation
857 in *Streptococcus pneumoniae*. *PLoS Pathogens* **9**:e1003473. doi:10.1371/journal.ppat.1003473

858 Lee MS, Seok C, Morrison DA. 1998. Insertion-duplication mutagenesis in *Streptococcus pneumoniae*: Targeting
859 fragment length is a critical parameter in use as a random insertion tool. *Applied and Environmental*
860 *Microbiology* **64**:4796–4802. doi:10.1128/aem.64.12.4796-4802.1998

861 Letunic I, Bork P. 2021. Interactive tree of life (iTOL) v5: An online tool for phylogenetic tree display and
862 annotation. *Nucleic Acids Research* **49**:W293–W296. doi:10.1093/nar/gkab301

863 Li H. 2018. Minimap2: Pairwise alignment for nucleotide sequences. *Bioinformatics* **34**:3094–3100.
864 doi:10.1093/bioinformatics/bty191

865 Li H. 2016. Minimap and miniasm: Fast mapping and de novo assembly for noisy long sequences. *Bioinformatics*
866 **32**:2103–2110. doi:10.1093/bioinformatics/btw152

867 Li H. 2011. A statistical framework for SNP calling, mutation discovery, association mapping and population
868 genetical parameter estimation from sequencing data. *Bioinformatics* **27**:2987–2993.
869 doi:10.1093/bioinformatics/btr509

870 Li H, Handsaker B, Wysoker A, Fennell T, Ruan J, Homer N, Marth G, Abecasis G, Durbin R, 1000 Genome Project
871 Data Processing Subgroup. 2009. The Sequence Alignment/Map format and SAMtools. *Bioinformatics*
872 **25**:2078–2079. doi:10.1093/bioinformatics/btp352

873 Lisboa J, Andreani J, Sanchez D, Boudes M, Collinet B, Liger D, Tilbeurgh H van, Guérois R, Quevillon-Cheruel S.
874 2014. Molecular determinants of the DprA-RecA interaction for nucleation on ssDNA. *Nucleic Acids*
875 *Research* **42**:7395–7408. doi:10.1093/nar/gku349

876 Liu X, Li JW, Feng Z, Luo Y, Veening JW, Zhang JR. 2017. Transcriptional repressor PtvR regulates phenotypic
877 tolerance to vancomycin in *Streptococcus pneumoniae*. *Journal of Bacteriology* **199**:54–71.
878 doi:10.1128/JB.00054-17

879 Madeira F, Park Y mi, Lee J, Buso N, Gur T, Madhusoodanan N, Basutkar P, Tivey ARN, Potter SC, Finn RD, Lopez
880 R. 2019. The EMBL-EBI search and sequence analysis tools APIs in 2019. *Nucleic Acids Research* **47**:W636–
881 W641. doi:10.1093/nar/gkz268

882 Manso AS, Chai MH, Atack JM, Furi L, De Ste Croix M, Haigh R, Trappetti C, Ogunniyi AD, Shewell LK, Boitano M,
883 Clark TA, Korlach J, Blades M, Mirkes E, Gorban AN, Paton JC, Jennings MP, Oggioni MR. 2014. A random

884 six-phase switch regulates pneumococcal virulence via global epigenetic changes. *Nature Communications*
885 **5**:1–9. doi:10.1038/ncomms6055

886 Marie L, Rapisarda C, Morales V, Bergé M, Perry T, Soulet AL, Gruget C, Remaut H, Fronzes R, Polard P. 2017.
887 Bacterial RadA is a DnaB-Type helicase interacting with RecA to promote bidirectional D-loop extension.
888 *Nature Communications* **8**:1–14. doi:10.1038/ncomms15638

889 Martin B, Garcia P, Castanié M-P, Claverys J-P. 1995. The recA gene of *Streptococcus pneumoniae* is part of a
890 competence-induced operon and controls lysogenic induction. *Molecular Microbiology* **15**:367–379.
891 doi:10.1111/j.1365-2958.1995.tb02250.x

892 Martin B, Soulet AL, Mirouze N, Prudhomme M, Mortier-Barrière I, Granadel C, Noirot-Gros MF, Noirot P, Polard
893 P, Claverys JP. 2013. ComE/ComE∼P interplay dictates activation or extinction status of pneumococcal X-
894 state (competence). *Molecular Microbiology* **87**:394–411. doi:10.1111/mmi.12104

895 Matthey N, Stutzmann S, Stoudmann C, Guex N, Iseli C, Blokesch M. 2019. Neighbor predation linked to natural
896 competence fosters the transfer of large genomic regions in *Vibrio cholerae*. *eLife* **8**.
897 doi:10.7554/eLife.48212

898 Mazin A v, Kowalczykowski SC. 1996. The specificity of the secondary DNA binding site of RecA protein defines
899 its role in DNA strand exchange. *Proceedings of the National Academy of Sciences of the United States of*
900 *America* **93**:10673–10678. doi:10.1073/pnas.93.20.10673

901 Mirouze N, Bergé MA, Soulet AL, Mortier-Barrière I, Quentin Y, Fichant G, Granadel C, Noirot-Gros MF, Noirot P,
902 Polard P, Martin B, Claverys JP. 2013. Direct involvement of DprA, the transformation-dedicated RecA
903 loader, in the shut-off of pneumococcal competence. *Proceedings of the National Academy of Sciences of*
904 *the United States of America* **110**. doi:10.1073/pnas.1219868110

905 Morrison DA, Guild WR. 1972. Transformation and deoxyribonucleic acid size: extent of degradation on entry
906 varies with size of donor. *Journal of bacteriology* **112**:1157–1168. doi:10.1128/jb.112.3.1157-1168.1972

907 Morrison DA, Mortier-Barrière I, Attaiech L, Claverys JP. 2007. Identification of the major protein component of
908 the pneumococcal eclipse complex. *Journal of Bacteriology* **189**:6497–6500. doi:10.1128/JB.00687-07

909 Mortier-Barriere I, Humbert O, Martin B, Prudhomme M, Claverys JP. 1997. Control of recombination rate during
910 transformation of *Streptococcus pneumoniae*: An overview. *Microbial Drug Resistance* **3**:233–242.
911 doi:10.1089/mdr.1997.3.233

912 Mortier-Barrière I, Velten M, Dupaigne P, Mirouze N, Piétrement O, McGovern S, Fichant G, Martin B, Noirot P,
913 le Cam E, Polard P, Claverys JP. 2007. A Key Presynaptic Role in Transformation for a Widespread Bacterial
914 Protein: DprA Conveys Incoming ssDNA to RecA. *Cell* **130**:824–836. doi:10.1016/j.cell.2007.07.038

915 Münch D, Roemer T, Lee SH, Engeser M, Sahl HG, Schneider T. 2012. Identification and in vitro Analysis of the
916 GatD/MurT Enzyme-Complex Catalyzing Lipid II Amidation in *Staphylococcus aureus*. *PLOS Pathogens*
917 **8**:e1002509. doi:10.1371/JOURNAL.PPAT.1002509

918 Nurk S, Bankevich A, Antipov D, Gurevich A, Korobeynikov A, Lapidus A, Prjibelsky A, Pyshkin A, Sirotkin A,
919 Sirotkin Y, Stepanauskas R, McLean J, Lasken R, Clingenpeel SR, Woyke T, Tesler G, Alekseyev MA, Pevzner
920 PA. 2013. Assembling genomes and mini-metagenomes from highly chimeric reads.In: Deng M., Jiang R.,
921 Sun F., Zhang X. (Eds) Research in Computational Molecular Biology. Springer, Berlin, Heidelberg. pp. 158–
922 170. doi:10.1007/978-3-642-37195-0_13

923 O'Brien KL, Wolfson LJ, Watt JP, Henkle E, Deloria-Knoll M, McCall N, Lee E, Mulholland K, Levine OS, Cherian T.
924 2009. Burden of disease caused by *Streptococcus pneumoniae* in children younger than 5 years: global
925 estimates. *The Lancet* **374**:893–902. doi:10.1016/S0140-6736(09)61204-6

926 Piotrowski A, Luo P, Morrison DA. 2009. Competence for Genetic Transformation in *Streptococcus pneumoniae*:
927 Termination of Activity of the Alternative Sigma Factor ComX Is Independent of Proteolysis of ComX and
928 ComW. *Journal of Bacteriology* **191**:3359. doi:10.1128/JB.01750-08

929 Price MN, Dehal PS, Arkin AP. 2009. Fasttree: Computing large minimum evolution trees with profiles instead of
930 a distance matrix. *Molecular Biology and Evolution* **26**:1641–1650. doi:10.1093/molbev/msp077

931 Quevillon-Cheruel S, Campo N, Mirouze N, Mortier-Barrière I, Brooks MA, Boudes M, Durand D, Soulet AL, Lisboa
932 J, Noirot P, Martin B, van Tilbeurgh H, Noirot-Gros MF, Claverys JP, Polard P. 2012. Structure-function
933 analysis of pneumococcal DprA protein reveals that dimerization is crucial for loading RecA recombinase
934 onto DNA during transformation. *Proceedings of the National Academy of Sciences of the United States of*
935 *America* **109**:E2466–E2475. doi:10.1073/pnas.1205638109

936 Rosenthal AL, Lacks SA. 1980. Complex structure of the membrane nuclease of *Streptococcus pneumoniae*
937 revealed by two-dimensional electrophoresis. *Journal of Molecular Biology* **141**:133–146.
938 doi:10.1016/0022-2836(80)90381-2

939 Ruan J, Li H. 2020. Fast and accurate long-read assembly with wtdbg2. *Nature Methods* **17**:155–158.
940 doi:10.1038/s41592-019-0669-3

941 Salvadori G, Junges R, Morrison DA, Petersen FC. 2019. Competence in *Streptococcus pneumoniae* and close
942 commensal relatives: Mechanisms and implications. *Frontiers in Cellular and Infection Microbiology*.
943 doi:10.3389/fcimb.2019.00094

944 Scheffers D-J, Pinho MG. 2005. Bacterial Cell Wall Synthesis: New Insights from Localization Studies.
945 *Microbiology and Molecular Biology Reviews* **69**:585–607. doi:10.1128/mmbr.69.4.585-607.2005

946 Sedlazeck FJ, Rescheneder P, Smolka M, Fang H, Nattestad M, von Haeseler A, Schatz MC. 2018. Accurate
947 detection of complex structural variations using single-molecule sequencing. *Nature Methods* **15**:461–468.
948 doi:10.1038/s41592-018-0001-7

949 Seemann T. 2019. GitHub - tseemann/barrnap: Bacterial ribosomal RNA predictor. *GitHub*.
950 https://github.com/tseemann/barrnap

951 Seemann T. 2014. Prokka: Rapid prokaryotic genome annotation. *Bioinformatics* **30**:2068–2069.
952 doi:10.1093/bioinformatics/btu153

953 Shak JR, Vidal JE, Klugman KP. 2013. Influence of bacterial interactions on pneumococcal colonization of the
954 nasopharynx. *Trends in microbiology* **21**:129–35. doi:10.1016/j.tim.2012.11.005

955 Shockley TE, Hotchkiss RD. 1970. Stepwise introduction of transformable penicillin resistance in Pneumococcus.
956 *Genetics* **64**:397–408. doi:10.1093/genetics/64.3-4.397

957 Sibold C, Henrichsen J, König A, Martin C, Chalkley L, Hakenbeck R. 1994. Mosaic *pbpX* genes of major clones of
958 penicillin-resistant *Streptococcus pneumoniae* have evolved from *pbpX* genes of a penicillin-sensitive
959 *Streptococcus oralis*. *Molecular Microbiology* **12**:1013–1023. doi:10.1111/j.1365-2958.1994.tb01089.x

960 Slager J, Aprianto R, Veening JW. 2019. Refining the pneumococcal competence regulon by RNA sequencing.
961 *Journal of Bacteriology* **201**:e00780-18. doi:10.1128/JB.00780-18

962 Slager J, Aprianto R, Veening JW. 2018. Deep genome annotation of the opportunistic human pathogen
963 *Streptococcus pneumoniae* D39. *Nucleic Acids Research* **46**:9971–9989. doi:10.1093/nar/gky725

964 Slager J, Kjos M, Attaiech L, Veening JW. 2014. Antibiotic-induced replication stress triggers bacterial
965 competence by increasing gene dosage near the origin. *Cell* **157**:395–406. doi:10.1016/j.cell.2014.01.068

966 Smith AM, Klugman KP. 2001. Alterations in MurM, a cell wall muropeptide branching enzyme, increase high-
967 level penicillin and cephalosporin resistance in *Streptococcus pneumoniae*. *Antimicrobial Agents and*
968 *Chemotherapy* **45**:2393–2396. doi:10.1128/AAC.45.8.2393-2396.2001

969 Stanhope MJ, Lefébure T, Walsh SL, Becker JA, Lang P, Pavinski Bitar PD, Miller LA, Italia MJ, Amrine-Madsen H.
970 2008. Positive selection in penicillin-binding proteins 1a, 2b, and 2x from *Streptococcus pneumoniae* and
971 its correlation with amoxicillin resistance development. *Infection, Genetics and Evolution* **8**:331–339.
972 doi:10.1016/J.MEEGID.2008.02.001

973 Straume D, Stamsås GA, Håvarstein LS. 2015. Natural transformation and genome evolution in *Streptococcus*
974 *pneumoniae*. *Infection, Genetics and Evolution* **33**:371–380. doi:10.1016/j.meegid.2014.10.020

975 Torres R, Serrano E, Alonso JC. 2019. Bacillus subtilis RecA interacts with and loads RadA/Sms to unwind
976 recombination intermediates during natural chromosomal transformation. *Nucleic Acids Research*
977 **47**:9198–9215. doi:10.1093/nar/gkz647

978 Walker BJ, Abeel T, Shea T, Priest M, Abouelliel A, Sakthikumar S, Cuomo CA, Zeng Q, Wortman J, Young SK, Earl
979 AM. 2014. Pilon: An integrated tool for comprehensive microbial variant detection and genome assembly
980 improvement. *PLoS ONE* **9**:e112963. doi:10.1371/journal.pone.0112963

981 Wang H, Marcišauskas S, Sánchez BJ, Domenzain I, Hermansson D, Agren R, Nielsen J, Kerkhoven EJ. 2018. RAVEN
982 2.0: A versatile toolbox for metabolic network reconstruction and a case study on *Streptomyces coelicolor*.
983 *PLoS Computational Biology* **14**:e1006541. doi:10.1371/journal.pcbi.1006541

984 Ween O, Gaustad P, Håvarstein LS. 1999. Identification of DNA binding sites for ComE, a key regulator of natural
985 competence in *Streptococcus pneumoniae*. *Molecular Microbiology* **33**:817–827. doi:10.1046/j.1365-
986 2958.1999.01528.x

987 Weng L, Piotrowski A, Morrison DA. 2013. Exit from Competence for Genetic Transformation in *Streptococcus*
988 *pneumoniae* Is Regulated at Multiple Levels. *PLoS ONE* **8**:e64197. doi:10.1371/journal.pone.0064197

989 Wick R. 2017. rrwick/Filtlong: quality filtering tool for long reads. *GitHub*. https://github.com/rrwick/Filtlong

990 Wick RR, Judd LM, Cerdeira LT, Hawkey J, Méric G, Vezina B, Wyres KL, Holt KE. 2021. Trycycler: consensus long-
991 read assemblies for bacterial genomes. *Genome Biology* **22**:1–17. doi:10.1186/s13059-021-02483-z

992 Wiktor J, Gynnå AH, Leroy P, Larsson J, Coceano G, Testa I, Elf J. 2021. RecA finds homologous DNA by reduced
993 dimensionality search. *Nature* **597**:426–429. doi:10.1038/s41586-021-03877-6

994 Wyres KL, Lambertsen LM, Croucher NJ, McGee L, von Gottberg A, Liñares J, Jacobs MR, Kristinsson KG, Beall
995 BW, Klugman KP, Parkhill J, Hakenbeck R, Bentley SD, Brueggemann AB. 2013. Pneumococcal capsular
996 switching: A historical perspective. *Journal of Infectious Diseases* **207**:439–449. doi:10.1093/infdis/jis703

997 Wyres KL, Lambertsen LM, Croucher NJ, McGee L, von Gottberg A, Liñares J, Jacobs MR, Kristinsson KG, Beall
998 BW, Klugman KP, Parkhill J, Hakenbeck R, Bentley SD, Brueggemann AB. 2012. The multidrug-resistant
999 PMEN1 pneumococcus is a paradigm for genetic success. *Genome Biology* **13**:R103. doi:10.1186/gb-2012-
1000 13-11-r103

1001 Yang H, Zhou C, Dhar A, Pavletich NP. 2020. Mechanism of strand exchange from RecA–DNA synaptic and D-loop
1002 structures. *Nature* **586**:801–806. doi:10.1038/s41586-020-2820-9

1003 Zhao G, Meier TI, Kahl SD, Gee KR, Blaszczak LC. 1999. BOCILLIN FL, a sensitive and commercially available
1004 reagent for detection of penicillin-binding proteins. *Antimicrobial Agents and Chemotherapy* **43**:1124–
1005 1128. doi:10.1128/aac.43.5.1124

1006

1007 ## Supplementary Tables

1008 **Table S1**: **Recombinant strains isolated in sequential rounds of transformation with AMX resistant DNA and**
1009 **their associated MICs**.

1010 **Table S2**: **Primers used in this study.**

1011 **Table S3**: **List of all recombination events identified in transformants using SNPs.**

1012 **Table S4**: **Summary statistics for the characterisation of SNP and recombination results for sequenced**
1013 **recombinant strains**. (A) All predicted events detected when compared to parent strain genome. Potential non-
1014 contiguity not accounted for. (B) Total DNA transferred during the final round of transformation for that strain.
1015 (*) All DNA or SNPs transferred into the original recipient (D39V or TIGR4), through one or two rounds of
1016 transformation (depending on the generation). SRA accession numbers for raw Illumina and PacBio reads used
1017 for analysis are also provided.

1018 **Table S5**: **Key amino acid substitutions in PBPs and MurM of recombinant strains**. Substitutions listed have
1019 been associated with β-lactam resistance in the literature previously. Cells coloured green have the same allele
1020 as D39V, those coloured blue have the same allele as 11A. Strain AMX MICs are also indicated for reference.

1021 **Table S6**: **Cloning design for fragments used to test for single-molecule non-contiguous recombination at the**
1022 ***pbp2x-mraY* locus**.

1023 **Table S7**: **Summary statistics from colonies isolated after transformation with different length and**
1024 **combinations of donor fragments to explain the occurrence of non-contiguous recombination.**

1025 **Table S8**: **SNPs detected in D39V^{M53}** .

1026 ## Supplementary Figures

1027 **Figure S1: Fluorescence and Coomassie stained images of Bocillin-FL gels**. (A) Bocillin-FL gel from Figure 3 and
1028 (B) gels from Figure 8.

1029 **Figure S2: Identification of non-contiguous recombination from sequenced recombinant strains using a**
1030 **bootstrapping method** (Croucher et al. 2012). (A) Scatter plot of distances between recombination events which
1031 were found to shorter than expected under a null hypothesis where events occur randomly around the
1032 chromosome. (B) Schematic showing how events were treated if they were found to be closer to each other
1033 than expected. (C) Histogram of recombination events length across all sequenced recombinant strains if non-
1034 contiguous recombination is not taken into account. (D) Histogram of recombination events length across all
1035 sequenced recombinant strains if non-contiguous recombination is accounted for.

1036 **Figure S3: Alignments of pbp2x-mraY from colonies isolated after transformation with different length and**
1037 **combinations of donor fragments to explain the occurrence of non-contiguous recombination.** Facets show
1038 colonies selected from different donor templates which correspond to Figure 6. Bases which match the recipient
1039 (D39V) are coloured grey, those which match the donor (11A) are shown in blue. (A) Long, (B) Up, (C) Down, (D)
1040 Up & Down, (E) Long-NH, (F) NH-Up, (G) Down-NH, and (H) NH-Up and Down-NH.

1041 **Figure S4: Dendrogram of strain relationships built from amino acid sequences of Pbp and murM proteins**.
1042 Alignments of Pbp1a, Pbp2b, Pbp2x, and MurM amino acid sequences were used to construct a phylogenetic
1043 tree of donor, recipient, and recombinant strains. AMX MICs are shown on the right, colour scale represents
1044 MIC and corresponds to figure 2, where yellow is an AMX MIC of 0.01 µg/mL and dark purple is an MIC of 4
1045 µg/mL.